AD-A119 534 HUGHES RESEARCH LABS MALIBU CA F/G 20/13
ELECTRONIC PROCESSES IN INP AND RELATED COMPOUNDS.(U)
JUL 82 K V VAIDYANATHAN, C L ANDERSON N00019-80-C-0619
UNCLASSIFIED NL

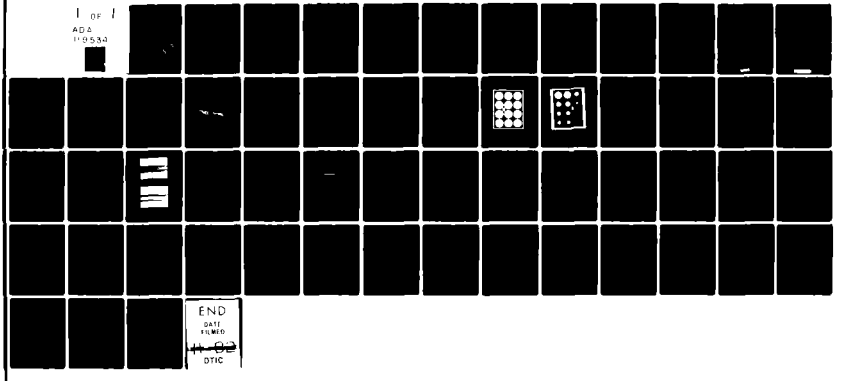

(12)

ELECTRONIC PROCESSES IN InP AND RELATED COMPOUNDS

K. V. Vaidyanathan, C. L. Anderson, H.L. Dunlap, and G. S. Kamath

Hughes Research Laboratories
3011 Malibu Canyon Road
Malibu, CA 90265

July 1982

N00019–80–C–0619
Final Report
For period 10 October 1980 through 9 October 1981

Sponsored by
DEPARTMENT OF THE NAVY
Naval Air Systems Command
Washington, D.C. 20361

UNCLASSIFIED

SECURITY CLASSIFICATION OF THIS PAGE (When Data Entered)

REPORT DOCUMENTATION PAGE		READ INSTRUCTIONS BEFORE COMPLETING FORM
1. REPORT NUMBER	2. GOVT ACCESSION NO. AD-A119534	3. RECIPIENT'S CATALOG NUMBER
4. TITLE (and Subtitle) ELECTRONIC PROCESSES IN InP AND RELATED COMPOUNDS		5. TYPE OF REPORT & PERIOD COVERED Final Report 10 Oct 1980 - 9 Oct 1981
		6. PERFORMING ORG. REPORT NUMBER
7. AUTHOR(s) K.V. Vaidyanathan, C.L. Anderson, H.L. Dunlap, and G.S. Kamath		8. CONTRACT OR GRANT NUMBER(s) N00019-80-C-0619
9. PERFORMING ORGANIZATION NAME AND ADDRESS Hughes Research Laboratories 3011 Malibu Canyon Road Malibu, CA 90265		10. PROGRAM ELEMENT, PROJECT, TASK AREA & WORK UNIT NUMBERS
11. CONTROLLING OFFICE NAME AND ADDRESS Department of the Navy Naval Air Systems Command Washington, D.C. 20361		12. REPORT DATE July 1982
		13. NUMBER OF PAGES
14. MONITORING AGENCY NAME & ADDRESS(if different from Controlling Office)		15. SECURITY CLASS. (of this report) UNCLASSIFIED
		15a. DECLASSIFICATION DOWNGRADING SCHEDULE

16. DISTRIBUTION STATEMENT (of this Report)

Approved for public release; distribution unlimited.

17. DISTRIBUTION STATEMENT (of the abstract entered in Block 20, if different from Report)

18. SUPPLEMENTARY NOTES

19. KEY WORDS (Continue on reverse side if necessary and identify by block number)

Ionization coefficient measurements
Liquid phase epitaxy of InP

20. ABSTRACT (Continue on reverse side if necessary and identify by block number)

The growth and characterization of high-purity epitaxial layers grown by liquid-phase-epitaxy (LPE) are described. Chemical and electrical evaluation of the layers indicate that silicon and sulfur are the dominant residual donors in LPE-grown InP layers. Techniques for controlling these dopants are discussed.

DD FORM 1 JAN 73 1473 EDITION OF 1 NOV 65 IS OBSOLETE

UNCLASSIFIED

SECURITY CLASSIFICATION OF THIS PAGE (When Data Entered)

The current-voltage characteristics of Schottky diodes on p-InP are analyzed. Aluminum, silver, and gold were tried as Schottky-barrier metals. The results reported here demonstrate that Al is the best choice as the Schottky metal. An automated system has been used to measure the relative photoresponse from Schottky diodes.

Photocurrent measurements due to pure electron and pure hole injection have been made as a function of bias applied to the sample. This data has been analyzed to yield ionization coefficients of electrons (α) and holes (β) in InP. The results clearly demonstrate that holes have a larger ionization coefficient than electrons in InP.

TABLE OF CONTENTS

LIST OF ILLUSTRATIONS

SECTION 1

INTRODUCTION

Developments in optical fibers have resulted in the availability of low loss, low dispersion fibers which can operate in the 1.0 to 1.6 μm wavelength range. These fibers are also radiation resistant and can be employed in communication systems operating in high radiation environment. They are expected to play a major role in the development of long base-line, high speed, secure, communication systems free of electromagnetic interference. To fully exploit this technology, it is necessary to develop semiconductor photoemitters (lasers and light emitting diodes) and photodetectors capable of operating in this wavelength range as well as amplifiers, logic circuits and other signal processing circuits. Examination of the fundamental semiconductor properties clearly indicates that $In_{(1-x)}Ga_xAs$ and $In_{(1-x)}Ga_xAs_{(1-y)}P_y$ compounds grown lattice-matched to InP substrates appear to be ideal candidates for such opto-electronic device applications.

Both avalanche photodiodes (APDs) and p-i-n diodes can be used as high speed photodetectors. The choice of a particular type of photodetector depends on the details of the system requirements. In the case of avalanche photodiodes, the relative magnitudes of the ionization coefficients of electrons (α) and holes (β) play an important role in the optimal design of these devices. The major goals of this experimental program are to develop techniques for measuring photomultiplied currents in suitable device structures, analyze the data to yield the ionization coefficients of electrons and holes as a function electric field in InP, and then later extend these measurements to the ternary and quaternary compounds.

The work that has been carried out under this progrm can be divided into the following areas:

- Growth of high purity InP epitaxial layers by liquid-phase epitaxy (LPE) using our patented infinite solution growth technique. We have characterized the chemical and electrical properties of such layers and have modified the growth system to facilitate the growth of ternary $In_{(1-x)}Ga_xAs$ layers.

- Development of device structures exhibiting abrupt reverse breakdown characteristics, free of microplasmas and exhibiting avalanche gains so that photocurrent measurements can be performed as a function of electric field. Since the electric field distribution is accurately known in Schottky barrier devices, we believe that these devices would be the most appropriate structures for performing these measurements. To develop such structures, we have investigated the current-voltage characteristics of Schottky diodes using different metals and have obtained barrier heights for these metals on p-type InP. The choice of p-InP is dictated because of unacceptably low Schottky barrier heights on n-type InP.

- Design and construction of an automated system capable of measuring photomultiplied currents due to pure electron- and pure hole-injection in the high-field region of the test structure. In this case, the electron- and hole-injection was obtained by illuminating the device from the backside with highly absorbing (0.6328 μm) and essentially transparent (1.152 μm) radiation, respectively. This procedure is advantageous since the same device structure is used to achieve the required carrier injections.

- Experimental measurement of photoinduced currents in these devices were performed as a function of the electric field. The data was analyzed to yield the ionization coefficients of electrons and holes in InP.

The report describes the progress made in each of these areas.

SECTION 2

EPITAXIAL GROWTH OF InP

InP, (In, Ga)As, and (In, Ga)(As, P) layers can be epitaxially grown by a variety of techniques such as liquid-phase epitaxy (LPE),[1] vapor phase epitaxy (VPE),[2] metal organic chemical vapor deposition (MOCVD),[3] planar reactive deposition (PRD),[4] and molecular beam epitaxy (MBE).[5] It appears that LPE offers the best potential for the growth of high-purity InP at this stage.

Two variations of the LPE technique are commonly used: the slide-bar technique using small solutions (the limited melt technique) and the dipping technique using larger solutions (the infinite solution technique). The slide-bar technique has the disadvantage that severe melt depletion effects can occur. Consequently, only a few layers with reproducible properties can be grown from a single melt. This may be a potential problem in the growth of ternary and quaternary layers. In contrast, the infinite solution technique, in principle, permits several hundred layers with reproducible properties to be grown from the same melt.

Hughes Research Laboratories (HRL) has developed a system which allows us to use a large solution to grow the epitaxial layers. The system illustrated in Figure 1, consists basically of an all-quartz growth tube connected by a high-vacuum valve to a stainless-steel entry chamber. A saturated solution of the appropriate elements contained in a crucible serves as the growth matrix. Once a specific solution has been prepared, it is kept in a palladium-purified hydrogen ambient and can be maintained at or near the growth temperature in a controlled environment for months. During a long series of runs, all operations, such as adding dopants or introducing substrates for epi-growth, are performed by passing these materials through an entry chamber, which can be independently evacuated and flushed with hydrogen before opening to the growth tube. It is also possible to maintain any other appropriate growth ambient while keeping all other variables under control. This capability is extremely useful in the growth of high purity InP layers and is discussed in detail later in this section.

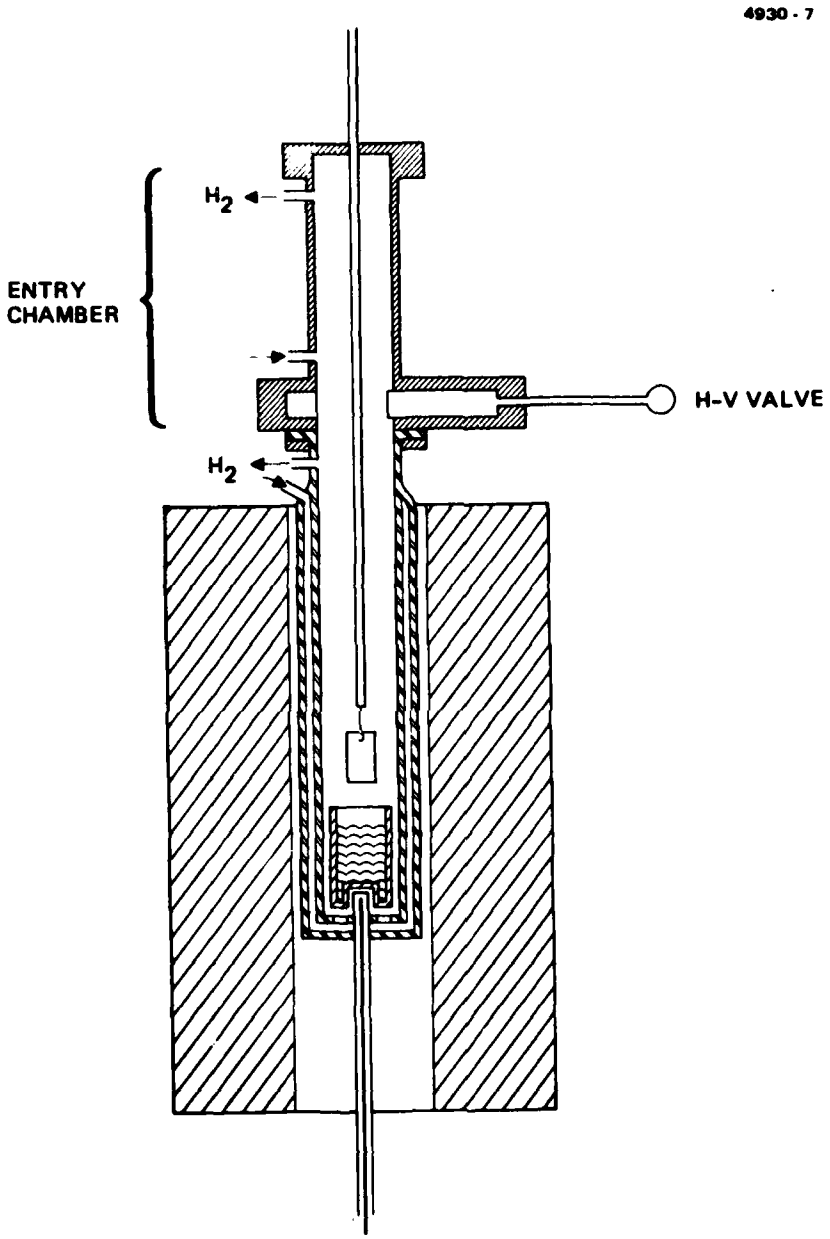

Figure 1. Schematic of LPE growth system.

The performance of opto-electronic devices depends critically on the ability to grow uniform, thin, homogeneous and dislocation-free epitaxial layers. Also, in devices involving heterojunctions, it is necessary to reduce defects at the interface. To satisfy all of these requirements, the surfaces must see a uniform growth ambient (a chemically homogeneous growth matrix and uniform temperature over the growth surface), and the layers must be grown slowly enough to permit near-equilibrium conditions to be established at the growth interface.

We have developed a graphite sample holder assembly to house the substrate (Figure 2) that permits us to grow the layers under such conditions. The substrate is introduced into the melt within the sample holder, and the whole assembly rotates in the melt until temperature equilibrium is fully established. This rotation further helps to ensure good mixing and homogeneity in the melt. By raising the graphite cover, the sample is exposed to the melt. Growth is stopped by (1) closing the cover; (2) raising the sample holder out of the solution; and (3) reopening the cover, at which point the solution that is trapped in the sample holder falls out. Note that at no time in the growth procedure does the surface of the sample pass through the meniscus on the solution. Furthermore, the cover of the sample holder does not wipe the melt from the sample. Using this technique, we have grown thin epitaxial layers with excellent surface morphology and reproducible electrical properties.

The infinite solution technique has been successfully used to grow high-purity InP layers with carrier concentrations of ~3 x 10^{15} cm^{-3} and mobilities of 4,500 cm^2 V^{-1} sec^{-1} (77°K mobility of 41,000 cm^2 V^{-1}) reproducibly. We have also conducted extensive studies, using internal funds, to study the influence of ~0.1 to 10 ppm of water vapor in the growth ambient. The results of this study summarized in Table 1 are quantitative in nature. They provide a good overall picture of the influence of water vapor in growth ambient but are not quantitative. These results can be explained as follows. Silicon is believed to be the dominant residual donor in InP. The quartz in the growth system reacts with H_2, which reduces it to SiO vapor. The SiO vapor is then reduced by In in solution, which results in Si doping of the solution. Consequently, in the presence of pure H, the Si level in solution reaches an equilibrium level. However, when a small quantity of water vapor is added to

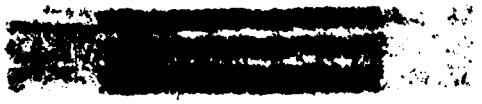

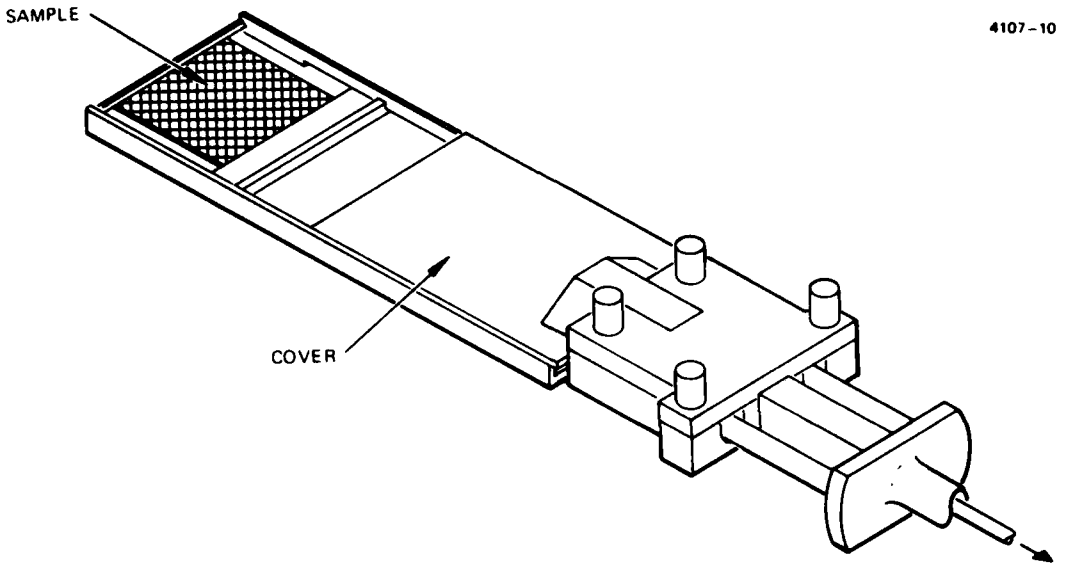

Figure 2. Graphite sample holder assembly.

[redacted]

Table 1. Electrical Properties of InP Epitaxial Layers Illustrating the Influence of Water Vapor in the Gas Stream

Sample Number	Ambient	n, cm^{-3} (300°K)	μ, $cm^2\ V^{-1}\ sec^{-1}$ (300°K)
1	Pure hydrogen	1.4×10^{17}	2600
2	Pure hydrogen	2.6×10^{17}	2600
3	Hydrogen + H_2O	2.1×10^{15}	3500
4	Hydrogen + H_2O	2.3×10^{15}	4500
5	Hydrogen + H_2O	4.2×10^{15}	4200
6	Hydrogen + H_2O	2.3×10^{15}	3800
7	Hydrogen + H_2O	2.5×10^{15}	4100
8	Hydrogen + H_2O	2.9×10^{15}	4100
9	Pure hydrogen	1.1×10^{16}	3700
10	Pure hydrogen	6.1×10^{16}	3100
11	Pure hydrogen	1.1×10^{17}	3200
12	Hydrogen + H_2O	2.3×10^{15}	4200

the growth ambient, the reduction of quartz by H is suppressed; also, the Si in solution reacts with water vapor, forming SiO vapors. Consequently, the Si level in solution is reduced considerbly. This model has been verified by experiments in which layers were grown by turning the water vapor on and off. Under those conditions, the net donor concentration cycles in the following manner: it is high when water vapor is absent and low when water vapor is present.

Extensive Hall-effect measurements have been performed as a function of temperature on the epitaxial layers. Analysis of the data yields the donor (N_D) and acceptor (N_A) concentrations and the degree of compensation. Analysis of the data shows that in layers grown in the presence of water vapor, both N_A and N_D decrease simultaneously. We believe that silicon is the only impurity in solution which is affected by water vapor. Consequently, we believe that our data indicates that silicon is an amphoteric dopant in InP.

The results of a low-temperature photoluminescence (PL) evaluation of InP epitaxial layers grown in the absence and presence of water vapor in the growth ambient are shown in Figure 3. The sample grown in pure H_2 had a total carrier concentration of 8.5×10^{16} cm^{-3}. The PL spectrum obtained from this sample is dominated by broad emission bands at 1.419 eV and 1.385 eV. The 1.419 eV band is related to band edge emission and is relatively broad in this sample. The emission at 1.385 eV appears to involve donors and acceptors. In contrast, the spectrum from a sample grown in the presence of water vapor exhibits a narrower edge emission (1.419 eV) and an absence of the donor-acceptor emission. The electrical and optical evaluations discussed above show that the samples grown in the presence of water vapor are, in fact, of higher purity than the ones grown in a H ambient (with no water vapor present).

We have also performed secondary ion mass spectrometry (SIMS) studies on InP liquid epilayers grown in H ambient, as well as in samples grown in the presence of water vapor. By using Cs ions as the primary bombarding species, it has been demonstrated that the detection sensitivity for Si and other group IV elements can be improved. As seen from the data in Figure 4, it is clear that layers grown in the presence of water vapor contain smaller quantities of Si as an impurity. Similar results were also obtained from Auger electron spectroscopy (AES) studies. The chemical studies mentioned above, in conjunction with the electrical data presented earlier, clearly demonstrate that the incorporation of Si resulting from the reduction of quartz is indeed an important source of donors in LPE-grown InP.

During the course of these investigations, we observed that not all solutions responded in the same fashion (quantitatively) to the addition of water vapor. Carrier concentrations $\sim$2 to 3×10^{16} cm^{-3} were measured when layers were grown from some solutions even in the presence of water vapor in the growth ambient. These results led us to believe that an additional donor may be present in the starting solution and consequently are incorporated in the grown layers. Detailed mass spectrometry analysis of such layers reveals the presence of considerable quantities of S. The S contamination may either be associated with the starting polycrystalline material or may be caused by some other source of contamination, such as the graphite sample holder.

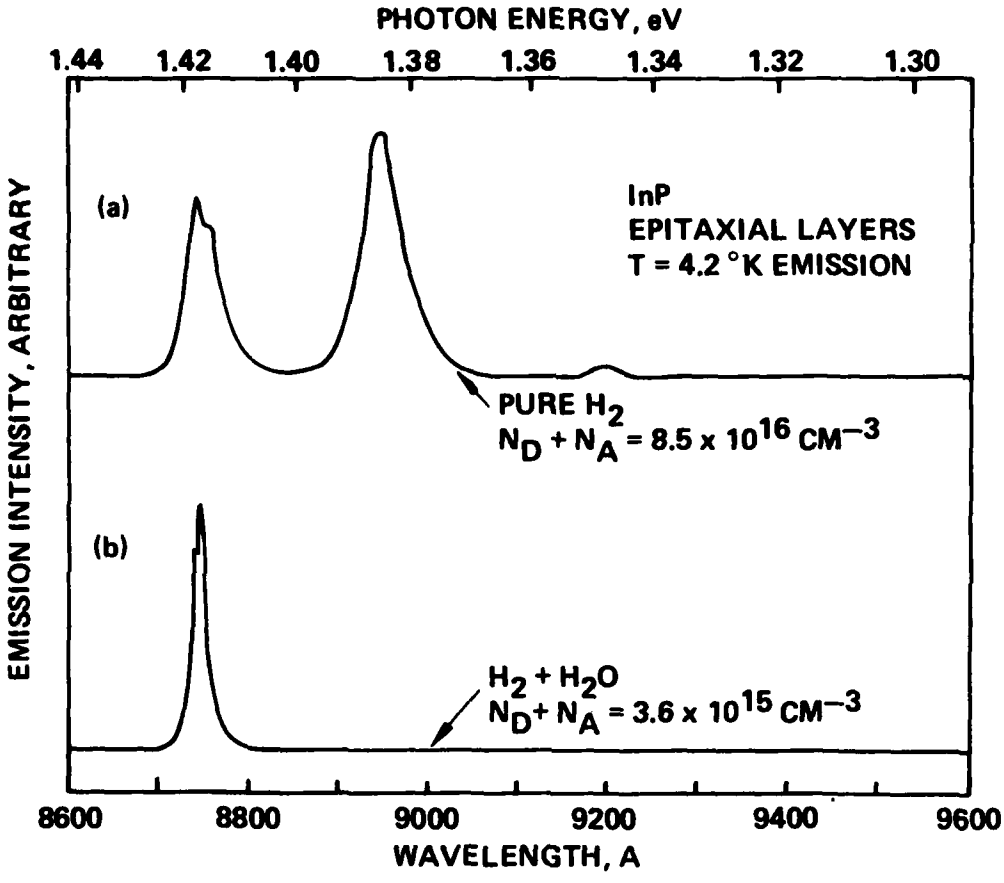

Figure 3. PL spectra of InP.

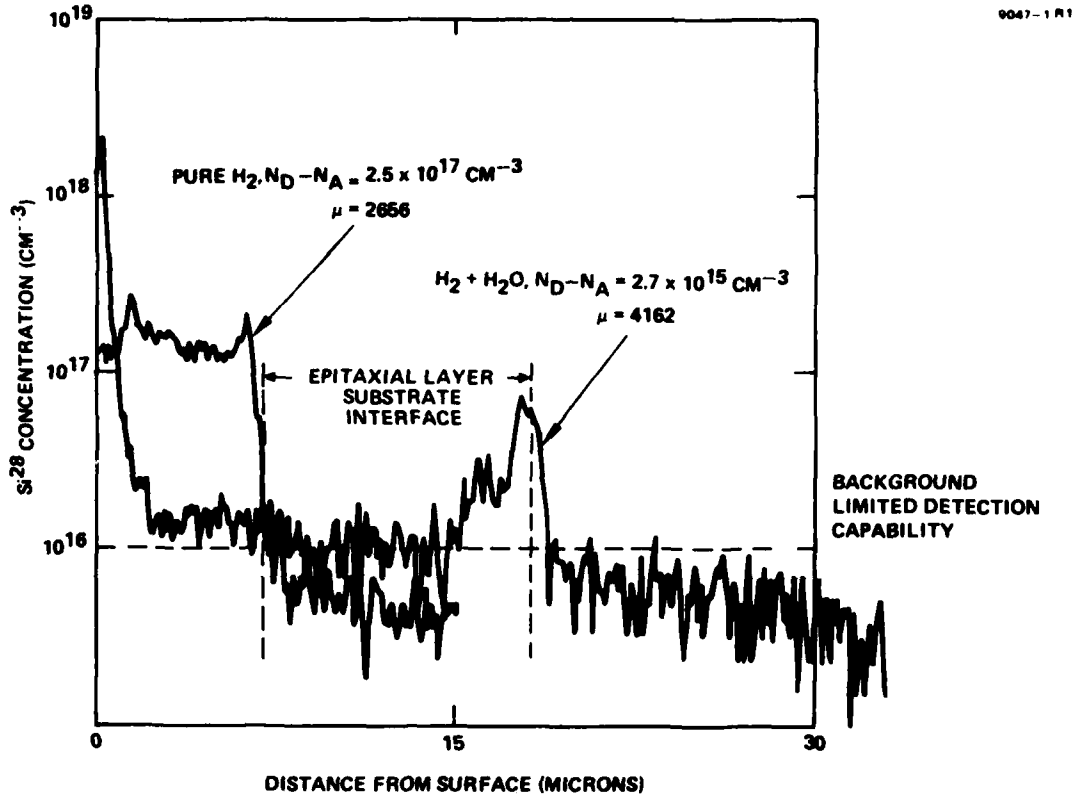

Figure 4. Secondary ion mass spectrometry (SIMS) profiles of silicon in InP epitaxial layers. Layer grown in the presence of water vapor contains small quantities of Si while a layer grown in pure hydrogen ambient contains large quantities of Si.

Since the vapor pressure of S is quite high, it is possible to reduce the S contamination by baking the growth solution at higher temperatures. Following such a bake-out, and by performing the growth at a temperature lower than the bakeout temperature in the presence of water vapor in the growth ambient, high purity InP layers can be grown even from a contaminated solution.

During the growth experiments discussed in the earlier section, we observed severe surface degradation of InP substrates. In the growth procedure, it is essential to maintain the substrate holder (with the substrate in the hydrogen ambient) above the solution in order to ensure that they have reached thermal equilibrium with the solution. This prewarming step is necessary to prevent spontaneous nucleation around the substrate holder on immersion into the solution. During such a prewarming step, we have observed severe surface degradation of InP substrates, primarily due to the loss of phosphorus. Such surface degradation can adversely affect the hetero-interface in the growth of InGaAs on InP. To avoid such interface problems, we have modified our sample holder allowing us to maintain an ambient of dilute phosphine over the sample. The ability to maintain such a controlled ambient over the sample during the warming cycle will prevent any loss of phosphorus and thus reduce surface degradation.

blank

SECTION 3

DEVICE STRUCTURE DEVELOPMENT

In the design of avalanche photodiodes, it is necessary to know the relative magnitude of the electron and hole ionization coefficients, $\alpha(E)$ and $\beta(E)$, respectively. The optimal design of avalanche photodiodes exhibiting high gain, and a large bandwidth with excellent signal-to-noise ratio, requires that the carrier with the highest ionization coefficient be photo-injected into the high field region to initiate avalanche multiplication.

The ionization coefficients effectively describe the interaction and multiplication of electrons and holes in the high field of the region of the semiconductor. It is essential that the device structures used for performing these measurements be capable of sustaining high electric fields and be free from local regions suffering from premature breakdown. It is also necessary that these devices be designed for efficient collection of light and the rapid transport of the photogenerated carriers to the high-field region of the device. Either Schottky barrier or p-n junction diodes can be used as suitable device structures. As pointed out earlier, breakdown resulting from inhomogeneities in the sample (microplasmas) or surface breakdown effects should be prevented in the device structure. Typically, surface breakdown effects can be minimized by suitable Schottky barrier guard rings or by shaping the mesas in mesa junction devices.

In addition to these requirements, Chynoweth[6] has pointed out some of the conditions to be satisfied in an ideal ionization coefficient measurement experiment:

- Pure electron or hole injection should be used in the same junction rather than complementary junctions.
- The profile and magnitude of the field in the junction region should be accurately known.
- The structures should be free from microplasmas over the bias range used in the measurements.

The first two of the Chynoweth criteria can be satisfied by using a Schottky barrier with appropriate optical injection of electrons and holes

in the high-field region of the device. The fabrication and properties of Schottky barrier device structures are described below.

To fabricate guarded Schottky diodes, we have designed a versatile yet simple mask set. Figure 5 shows the first level in this mask set. This mask will permit us to form ohmic contacts on the front surface of the device. After a photolithographic liftoff has been completed with this mask, the ohmic contact metal will cover the wafer except for the regions corresponding to the dark circles on the mask. Figure 6 shows the second level of the mask, which will permit us to define the Schottky barrier and the guard ring metalization in one photolithographic step. Two different spacings between the Schottky barrier and the guard ring (3 and 10 μm) are available. Also, diodes with diameters of 400, 200, 100 and 50 μm can be fabricated. Diodes with no guard ring are also available as test devices. By using an appropriate polarity of the mask shown in Figure 5, the region underneath the ohmic contact can be heavily doped by ion implantation while maintaining the doping level underneath the Schottky at acceptably low levels. There is also a provision for performing selective area implantation to form planar p-n junction structures by ion implantation. This feature will permit us to fabricate p^+-n or n^+-p junction diodes, along with the Schottky diodes as test structures.

Using the mask set discussed above, we have fabricated and evaluated Schottky diodes on p-type InP. The p-InP samples were lightly doped (>6 x 10^{15} holes/cm^3) and were obtained from Varian Associates. They were chemimechanically polished in a 2 percent solution of Br in methanol to yield smooth scratch-free surfaces. They were further free etched in a yield smooth scratch-free surfaces. They were further free etched in a solution of 1:1:1:6 perchloric acid (HClO:HCl:acetic acid (H Ac)):HNO_3. To ensure that low resistance ohmic contacts could be formed, the regions underneath the ohmic contacts were selectively ion implanted with beryllium. The samples were encapsulanted with phosphosilicate glass (PSG) and annealed at 700°C. The implantation doping process resulted in increasing the hole concentration underneath the contacts. Ohmic contacts were formed by sputter depositing Au-Zn alloy, patterning it and alloying it at 480°C for one minute. Schottky barrier diodes were fabricated by evaporating either Al, AG, or Au as the Schottky metal and their I-V characteristics were evaluated.

10672-1

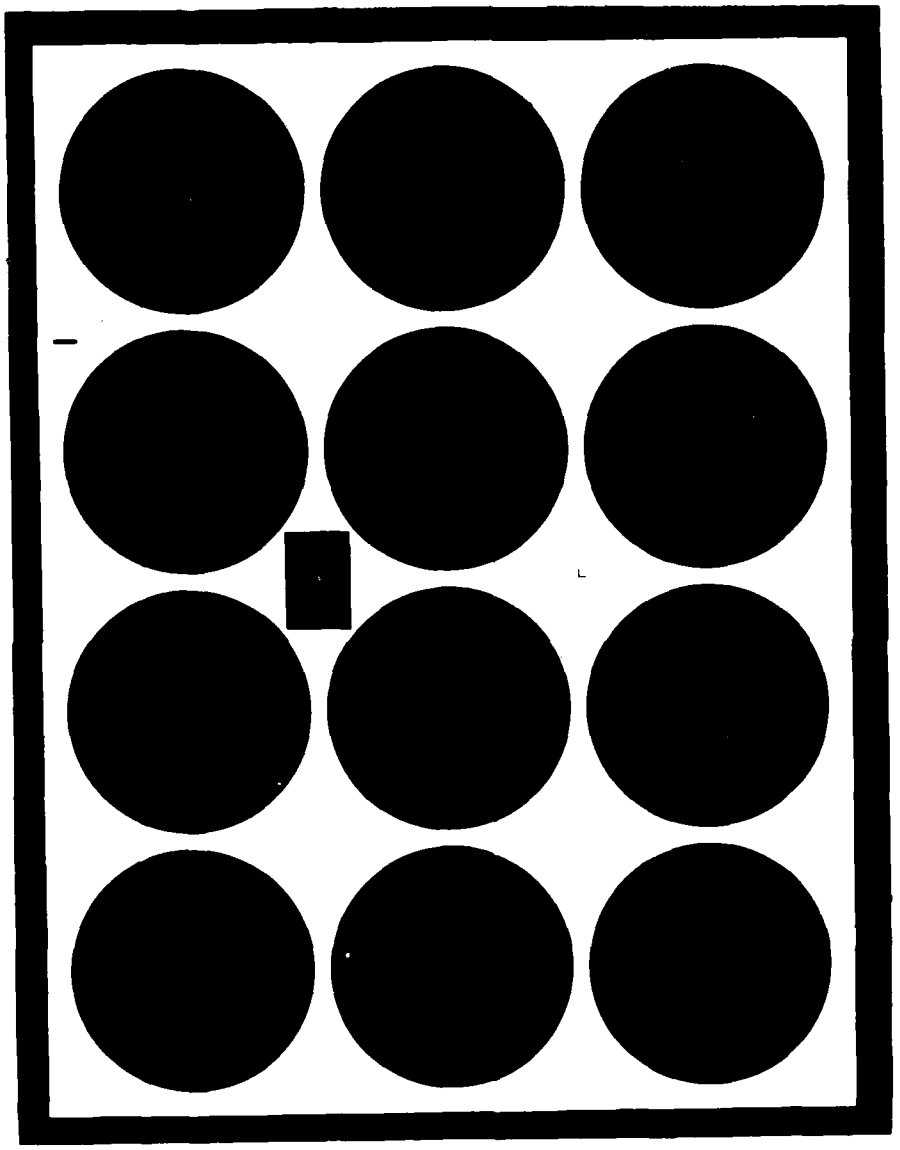

Figure 5. First level mask to define ohmic contacts for fabricating guarded Schottky diodes in InP.

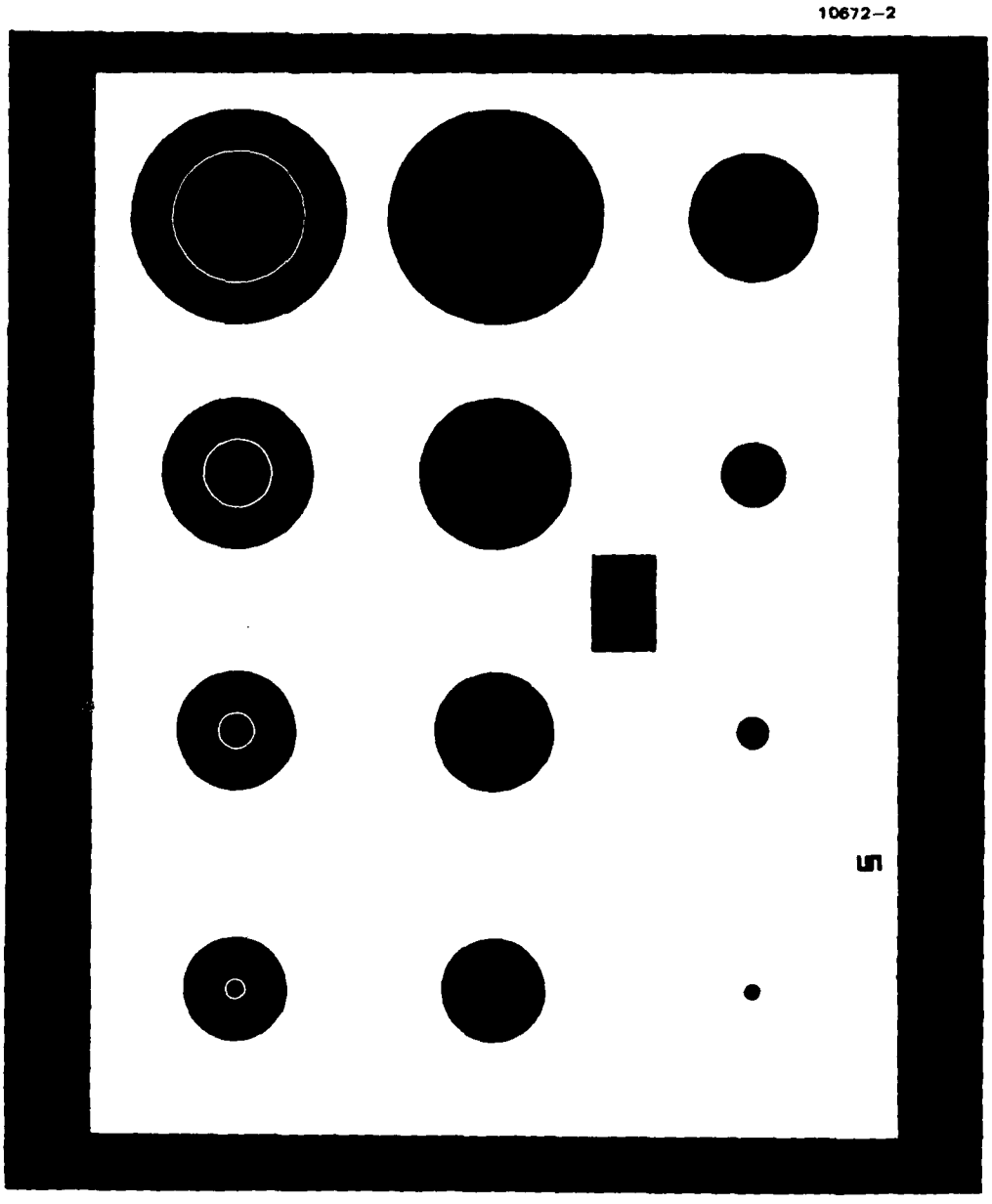

Figure 6. Second level mask to define the Schottky and guard ring in InP.

Figure 7 illustrates the I-V characteristics in the reverse direction of Al Schottky diodes on p-InP. The leakage current, as seen from the figure, is quite low, even at a reverse bias voltage of 20 V. The breakdown is abrupt, and there appears to be no problem associated with microplasmas. Even in the presence of external illumination, the reverse leakage current is quite low. The forward I-V characteristics obtained for Al Schottky diodes with different diameters is shown in Figure 8. The I-V curves can be described by the classic relation,

$$J = A^{*}T^{2}\, e^{\frac{q\phi_B}{kT}} \left[\exp\left(\frac{qV}{nkT}\right) - 1\right], \qquad (1)$$

where A^{*} is the Richardson's constant, T is the absolute temperature, $q\phi_B$ is the Schottky barrier height in eV, V is the applied voltage, and n is the ideality factor. For Al on p-InP, we estimate the Schottky barrier height to be 0.9 eV and the ideality factor to be 1.059. The I-V characteristics in thw forward direction for Au and Ag Schottky diodes are shown in Figures 9 and 10, respectively. Analysis of the data indicates that the Schottky barrier height of Au on p-InP is $\sim$0.64 eV, while the ideality factor is 1.3. Previously published data indicate that the barrier height of Au on p-InP may be $\sim$0.76 eV. For Ag, we estimate the barrier height to be between 0.74 and 0.81 eV, and the ideality factor to be $\sim$1.5.

We have also performed capacitance-voltage measurements as a function of reverse bias on these Schottky diodes. The barrier height estimated from eV measurements is in reasonable agreement with the values estimated from C-V measurements. We estimate the carrier concentration to be between 4×10^{16} cm^{-3} and 5×10^{16} cm^{-3} in the diodes studied. From this study, it is clear that Al forms an ideal Schottky barrier on p-InP. We therefore chose to use Al Schottky diodes as our test structure. Analysis of the data also reveals that the reverse leakage current scales with the area of the devices, indicating that the dominant mechanism is due to bulk leakage rather than surface effects.

To perform the ionization coefficient measurements, it is necessary to thin the samples so that almost all of the photogenerated carriers are injected into the high-field region and are not lost by recombination. Since the samples

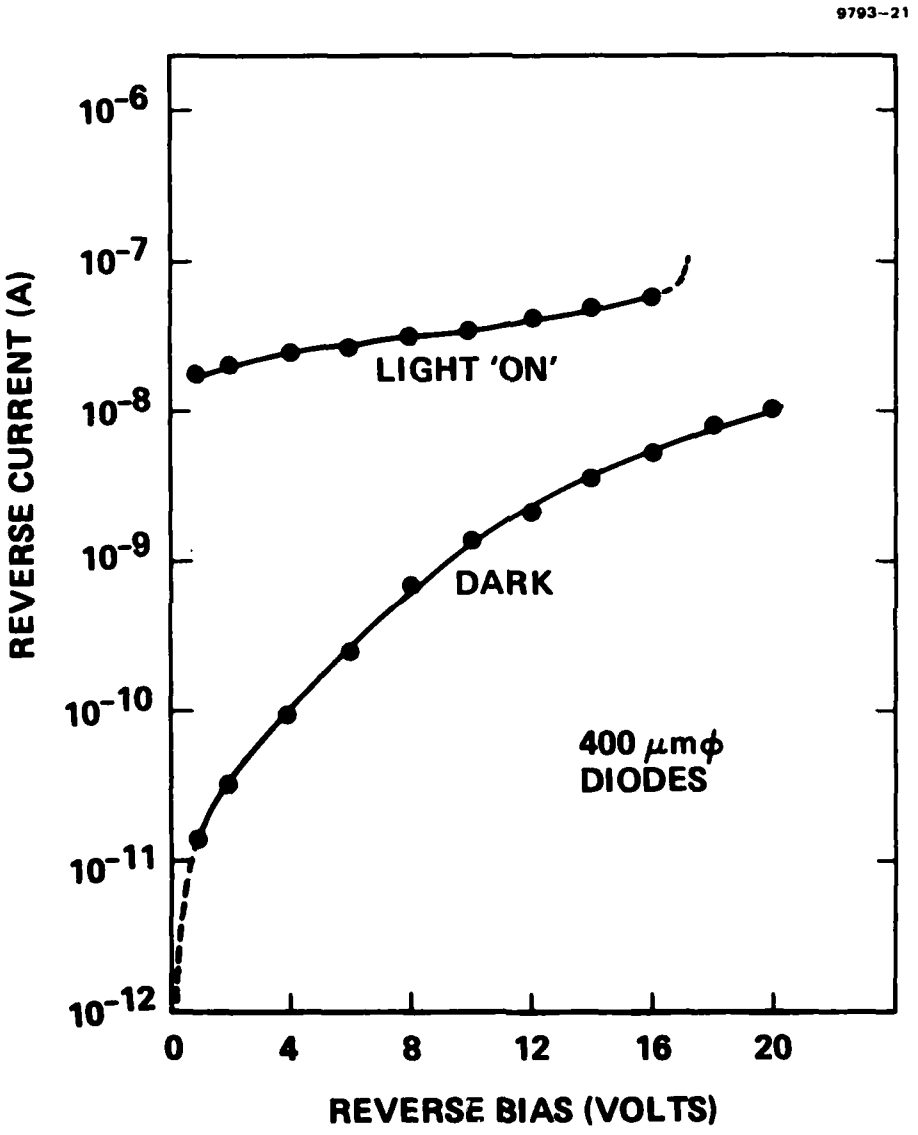

Figure 7. Current-voltage characteristics of 400-μm-diameter reverse-biased Schottky diodes on p-InP.

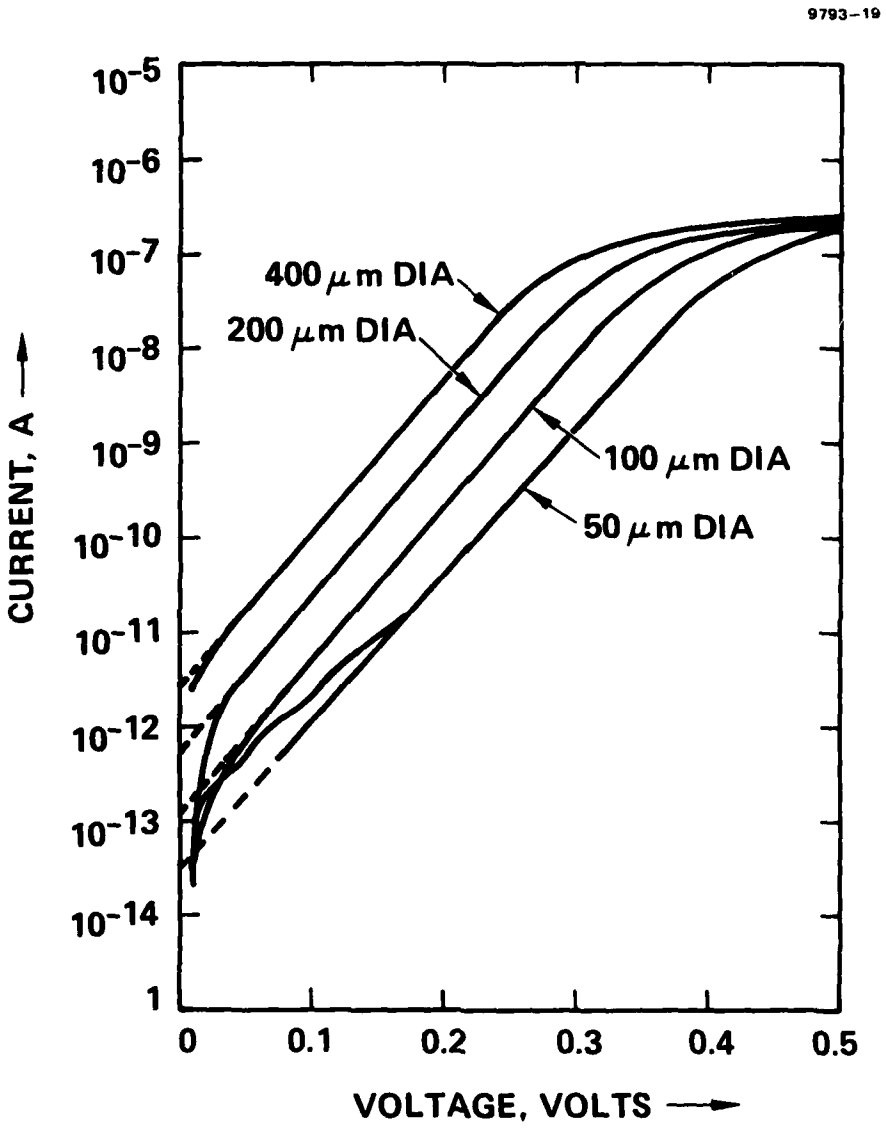

Figure 8. Current-voltage characteristics of forward-biased Schottky diodes on p-InP. The Schottky metal was Al.

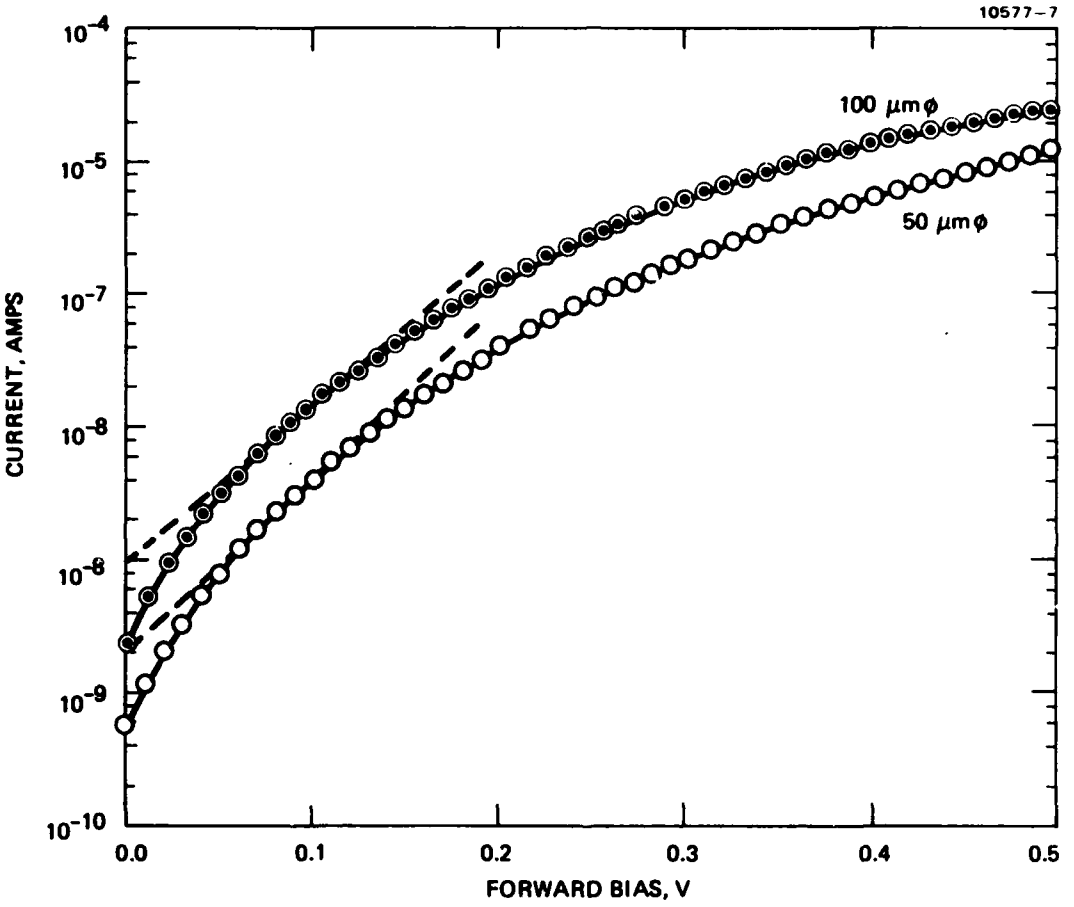

Figure 9. Current-voltage characteristics (forward bias) of Au Schottky diodes on p-InP.

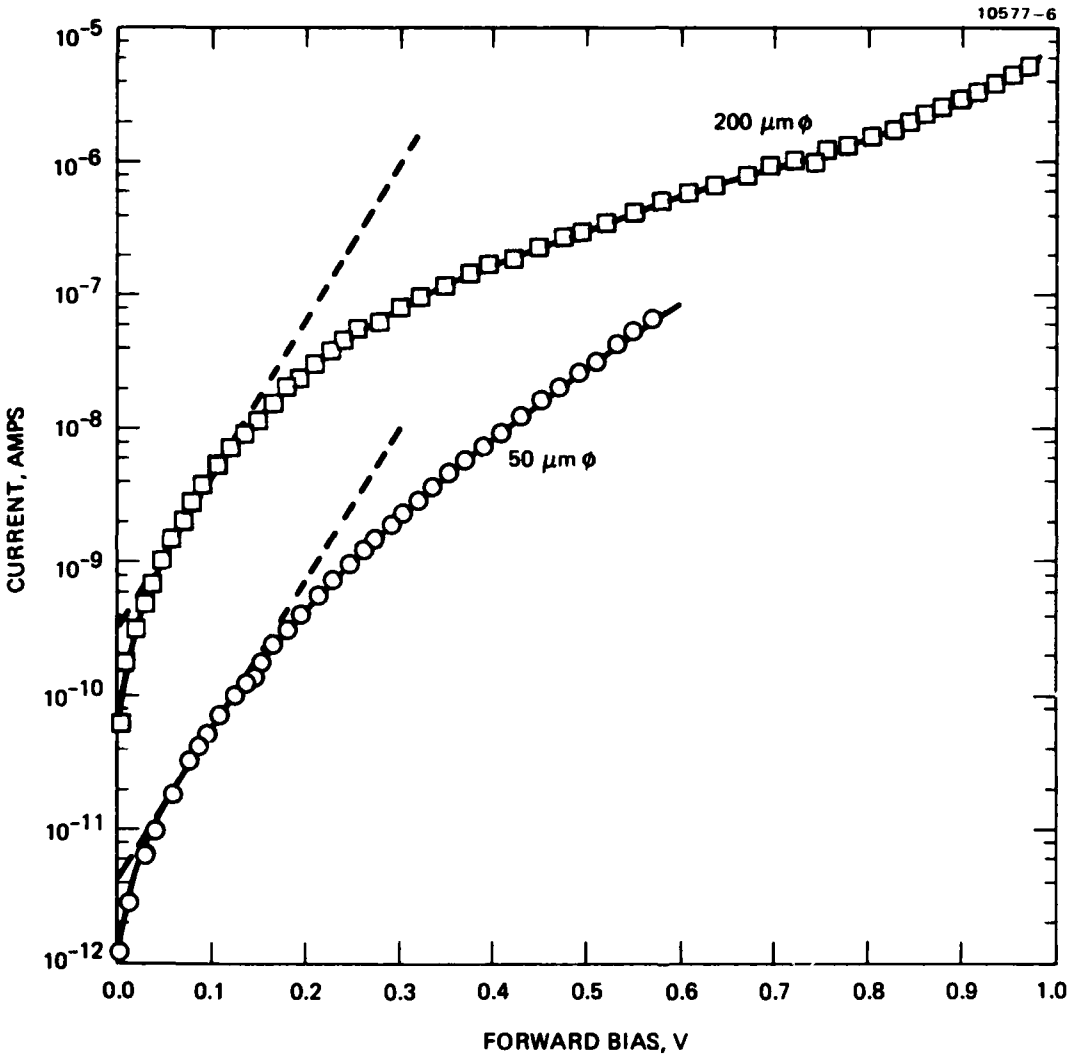

Figure 10. Current-voltage (forward) characteristics of Ag-Schottky diodes on p-InP.

have to be self-supporting, it is necessary to selectively thin a portion of the sample. When the sample is etched in a solution that is mechanically stirred or agitated, the typical etch region with a moat around the edge is obtained and is shown in Figure 11. However, when a jet of the etchant solution is directed at the sample a more uniform etching is obtained (Figure 12). But using a combination of jet etching and etching in an agitated solution appears to produce adequate thinning. We have used the above approaches using an etching solution of 2 percent bromine in methanol to thin InP samples.

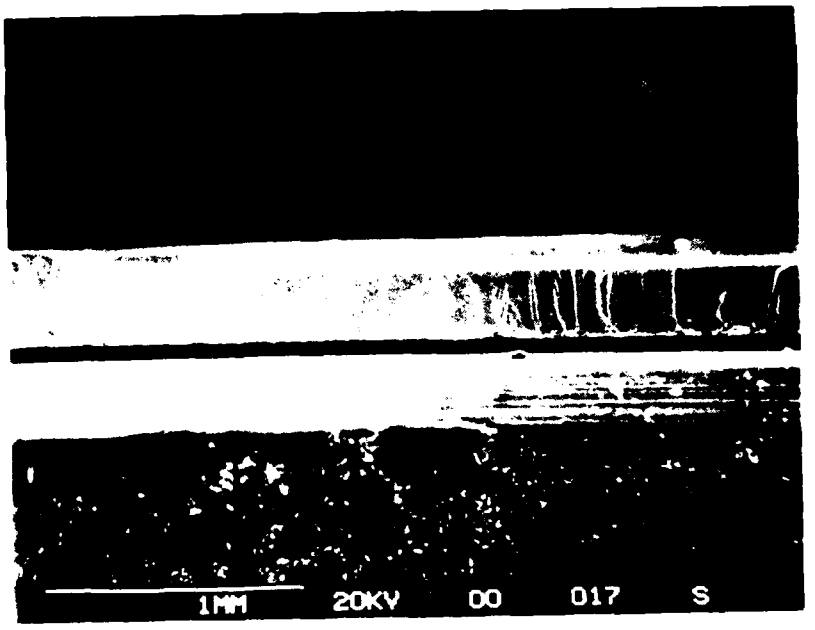

Figure 11. SEM micrograph of a mesa etch in InP with mechanically agaited 2% solution of bromine in methanol. "Moating" around the edge is clearly evident.

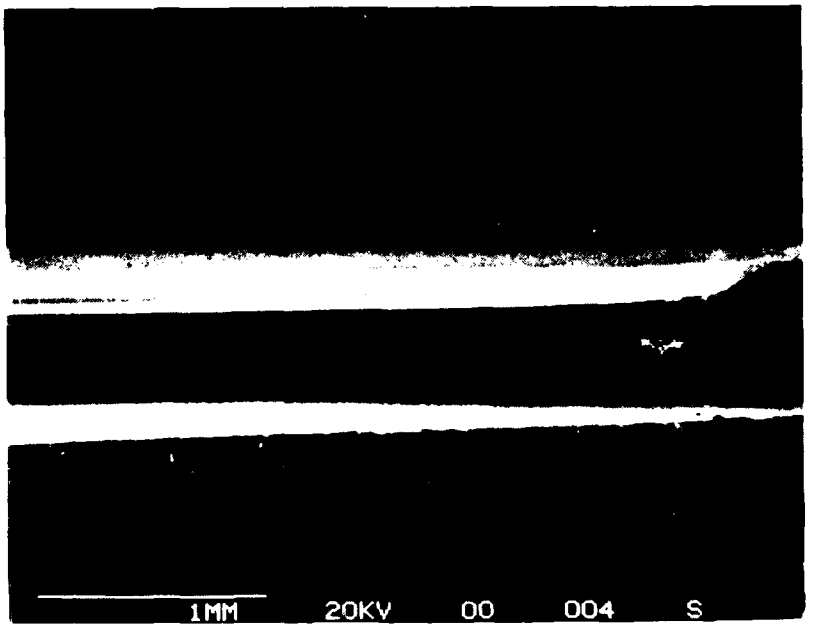

Figure 12. SEM micrograph of a mesa in InP produced by jet thinning with 2% solution of bromine in methanol. The edges are smooth with no evidence of moating.

blank

SECTION 4

IONIZATION COEFFICIENT MEASUREMENT SYSTEM

As discussed in an earlier section, an ideal ionization coefficient measurement experiment must be capable of achieving pure electron and hole injection in the same device rather than in complementary devices. Our experimental system has been designed to satisfy this criterion and does not require the use of a transparent Schottky barrier. The details of the experimental setup are described below.

The pure electron and pure hole injection in our case are achieved by the absorption of 0.638 and 1.152 μm radiations, respectively. The sample in both cases is illuminated from the backside, and the ohmic, as well as the Schottky contacts, are made from the top surface of the wafer. The 0.638 μm radiation, with energy greater than the band gap of InP, creates electron-hole pairs near the back surface of the sample, and the minority carriers (in our case, electrons) will be injected into the high-field region (provided that the sample is sufficiently thin), avalanche multiplied, and then collected by the reverse-based Schottky. The 1.152 μm radiation, on the other hand, is highly transparent, and consequently, is incident at the metal-semiconductor interface. As a result, holes are injected over the barrier, which in turn are injected onto the high-field region, thus achieving pure-electron and pure-hole injection.

The detailed experimental setup is shown in Figure 13. Two stable He-Ne lasers, one capable of operation at 0.6328 μm and the other at 1.152 μm, provide the necessary illumination. Chopped light from the two lasers is focused onto optical fibers, labeled 1 and 2 in Figure 13. The two fibers are fused in the middle, permitting coupling of radiation between the fibers. Approximately 50 percent of the radiation couples from fiber 1 to fiber 2 and vice versa. Radiation from fiber 2 is focused by a microscope objective onto the device structure, as shown in Figure 13. The radiation from fiber 1 is detected by a reference photodetector and provides a measure of the laser intensity incident on the test device at any given time. This feature will permit us to account for any fluctuations in the laser intensity during the

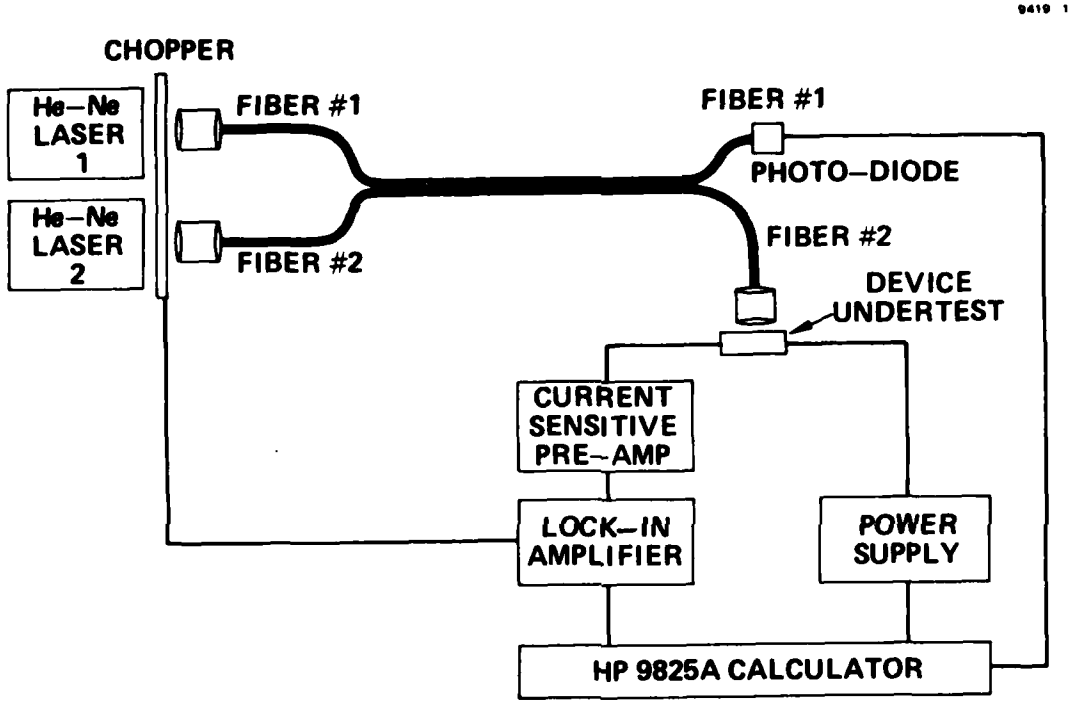

Figure 13. Schematic of the automated photoresponse measurement system.

time it takes to complete the measurement. The photo-induced currents will be measured by a current-sensitive preamplifier and a lock-in amplifier. The voltage applied to the device under test and the measurements will be controlled by an HP 9825A calculator.

The software necessary to perform the automated photocurrent measurements was developed. Figure 14 represents the logic flow chart diagram of the various programs developed to perform the measurements. Input data to be entered before commencing any photoresponse measurement include the maximum allowable bias voltage (V) applied to the sample, the maximum allowable photocurrent (I_{ph}), the incremental bias voltage (ΔV), minimum allowable incremental voltage (ΔV_{min}), and the maximum allowable increase in photocurrent for normal bias voltage change ($\Delta I_{ph_{max}}$). It is also possible to enter the sample number and wavelength of the laser used. After these data are entered, photocurrent measurements are performed (see Start, Foto program).

To begin with, a specified time constant (τ) is set on the lock-in amplifier. After every increase in bias voltage is made, the system waits for 20 time constants before mesuring the photocurrent. Ten such measurements of Iph are made. If the variations in photocurrent are equal to or more than 10 percent of the mean photocurrent, the time constant is increased and the procedure repeated. The laser power is also closely monitored to ensure that the laser intensity stays constant throughout the measurement cycle. After acceptable measurements are made, the data is printed out and also plotted. These automated measurements permit us to obtain smooth photocurrent measurements as a function of electric field.

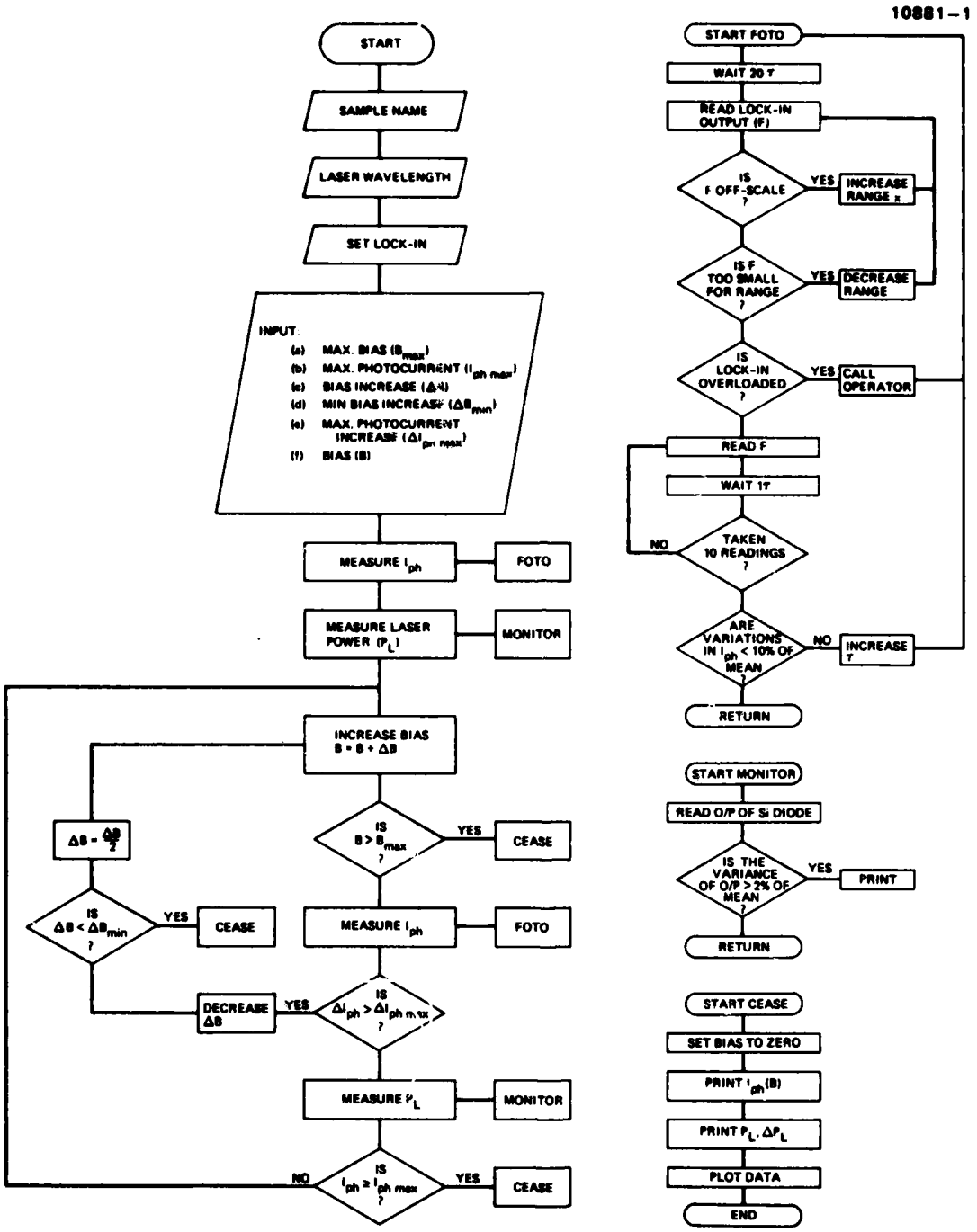

Figure 14. Flow chart of the software required to perform automated photoresponse measurements.

SECTION 5

IONIZATION COEFFICIENT MEASUREMENTS

A. INTRODUCTION

In order to evaluate the ionization coefficients for electrons (α) and holes (β), it is essential to measure photo-induced currents as a function of reverse bias under conditions af pure electron and pure hole injection into the high field region of devices which satisfy the criteria discussed in Section 3.

In this section, we discuss the theoretical expressions used to calculate the multiplication factors, Mn and Mp (due to electron and hole injection, respectively), and the analysis of the data to evaluate the ionization coefficients of electrons (α) and holes (β) for a uniformly doped depletion region.

B. THEORETICAL ANALYSIS

In order to obtain the multiplication factors Mn and Mp due to pure electron and pure hole injection fron the measured photocurrent data, it is necessary to estimate the base-line non-multiplied photocurrent as a function of reverse bias or electric field. The usual approach has been to use a linear extrapolation of the low field photocurrent as the base-line photocurrent. This linear extrapolation assumption usually overestimates the base-line photocurrent.

Recently, Woods et al[8] have fitted the low field nonmultiplied minority carrier initiated photocurrents in the case of silicon by considering photogeneration and minority carrier diffusion processes. Assuming that the sample under test is uniformly doped, Kao and Crowell[7] show that the minority carrier nonmultiplied photocurrent is given by,

$$I_L = \frac{I_o}{\mathrm{Cosh}(L/L_{np})} \quad , \tag{2}$$

where L is the thickness of the undepleted portion of the sample (shown in Figure 15), and L_{np} is the minority carrier diffusion length. Using either

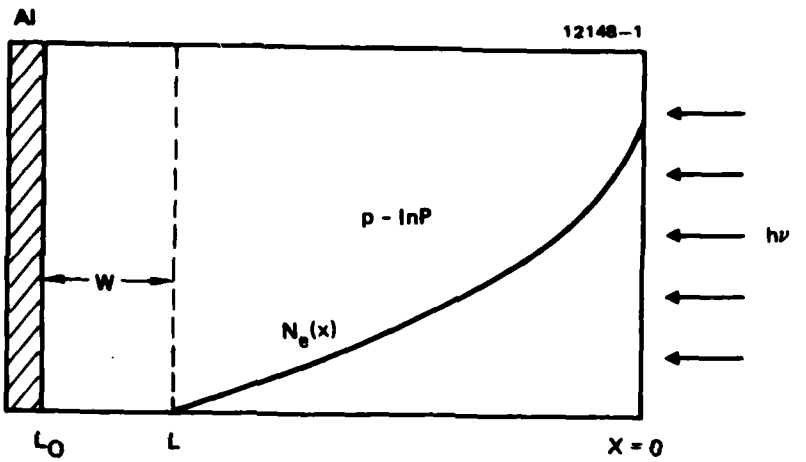

Figure 15.
Schematic diagram describing minority carrier diffusion process in a Schottky diode illuminated from the back side.

of the two approximations for the minority carrier initiated base-line photocurrents, it is possible to evaluate Mn as a function of reverse bias for the Schottky barrier test devices on p-InP.

In the case of majority carrier initiated photocurrents, Kao and Crowell[7] have shown that the photocurrent can be expressed as

$$I_{ph(baseline)} = k \langle \tau_{QMT} \rangle e^{-(Xm/\lambda e)} \tag{3}$$

where $\langle \tau_{QMT} \rangle$ is the Quantum mechanical transmission coefficient and does not vary appreciably over the range of electric field encountered in experimental measurements and k is a proportionality constant. In this expression, Xm represents the position of the potential barrier maximum from the metallurgical boundary due to image force potential. The value of Xm is given by,

$$Xm \simeq \left(\frac{q}{16\pi\epsilon_s Em}\right)^{\frac{1}{2}} , \tag{4}$$

where ϵ_s is the semiconductor permittivity, Em is the maximum value of the electric field, and λ_e is the effective mean free path for phonon scattering. The proportionality factor is a complex function of the incident light intensity, the barrier height, and the energy of the incident radiation. Since these parameters are not dependent on the value of the electric field, it is clear that the nonmultiplied photocurrent is a function of the electric field in the device.

Once the values of Mn and Mp have been determined for the case of pure electron and pure hole injection, α and β can be estimated as functions of electric field by the following expressions:[6,7]

$$\alpha(Em) = \frac{1}{Mp} \frac{d(\ln Mn)}{d\,Em} \cdot \frac{qNa}{\epsilon_s} \tag{5}$$

and

$$\beta(Em) = \alpha(Em) + \frac{d^{\ln\left(\frac{Mn}{Mp}\right)}}{dEm} \cdot \frac{qNa}{\epsilon_s} \tag{6}$$

In these, Em is the maximum electric field, Mp and Mn are the multiplication coefficents for majority and minority carier initiated multiplication events, N_a is the doping concentration in the p-type material, and ε_s is the permittivity of the semiconductor.

C. EXPERIMENTAL RESULTS

As discussed in Section 3, devices used for ionization coefficients should be free from microplasma and edge breakdown effects. Both of these effects result in anomalous photoresponse when illuminated with carrier injecting illumination and make it difficult to analyze photoresponse data to yield the ionization coefficients of electrons and holes. To ensure that the devices used in this study were free from such deleterious effects, we measured the relative photoresponse by scanning visible and IR radiations across the diode. Photoresponse from a typical diode for both visible and IR scans are shown in Figure 16. The photoresponse across the diode is uniform with no evidence of anamolous response. We, therefore, believe that those devices are from microplasma effects.

The measured photocurrent from a 400 μm diameter diode is shown in Figure 17 as a function of reverse bias. The solid curve was obtained by illuminating the diode with 1.152 μm radiation, corresponding to majority carrier injection condition. The dashed curve was obtained by illuminating the diode with 0.6328 μm radiation (minority carrier injection). There is no evidence of carrier multiplication in this data. The injected minority carriers have to be transported by diffusion to the high field region of the device. In the case of the thick sample, the injected minority carriers will recombine. Thus, in order to observe multiplication due to minority carriers, it is necessary to thin the sample. Using the technique discussed in Section 3, several devices were thinned in a solution of bromine in methanol. The measured photocurrent from a typical diode is shown in Figure 18 as a function of bias for various diode thicknesses. As the device is thinned, the measured photocurrent increases in magnitude; in the case of the thinnest diode, there is clear evidence of carrier multiplication at high values of bias.

In Figure 19, the normalized photoresponse from the 6-μm -thick diode (Figure 18) is plotted as a function of electric field. The normalization factor at any bias is defined as the ratio between the measured photocurrent at that bias voltage and the photocurrent at zero bias. The solid line

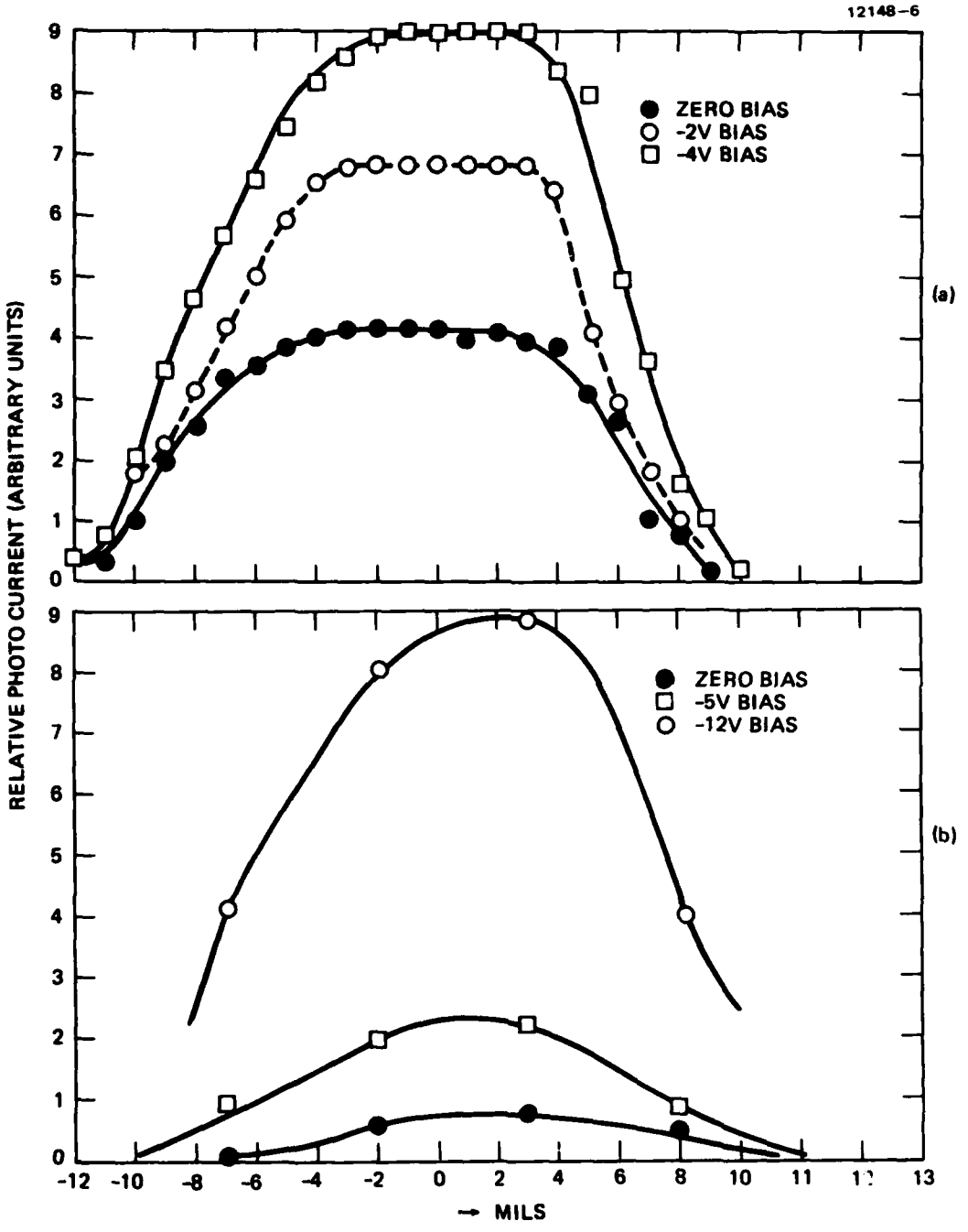

Figure 16. Relative photoresponse due to scanned incident radiation (a) visible scan (b) IR scan.

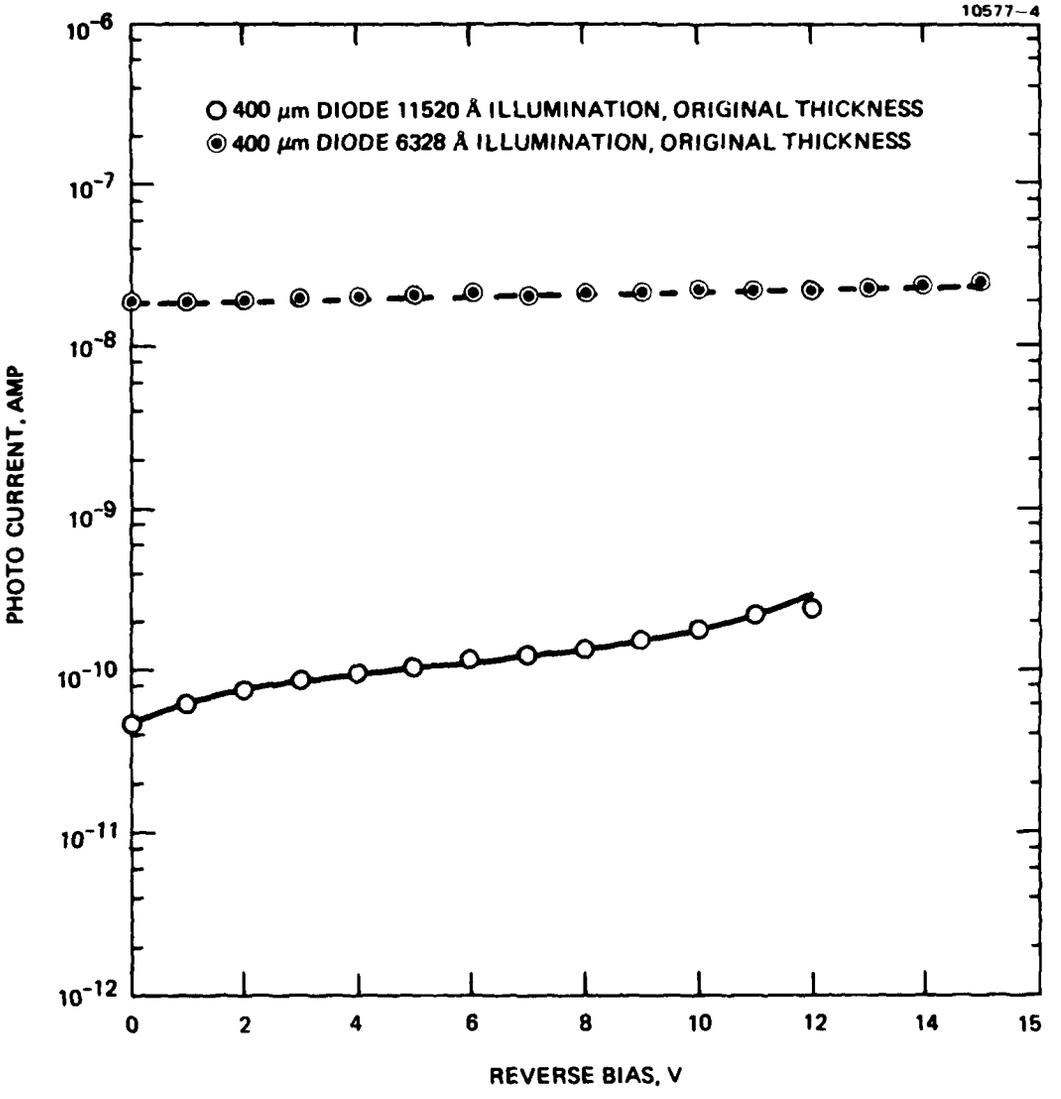

Figure 17.
The measured photocurrent as a function of reverse bias for both 0.6328 μm and 1.152 μm illumination obtained from a Schottky diode on p-InP.

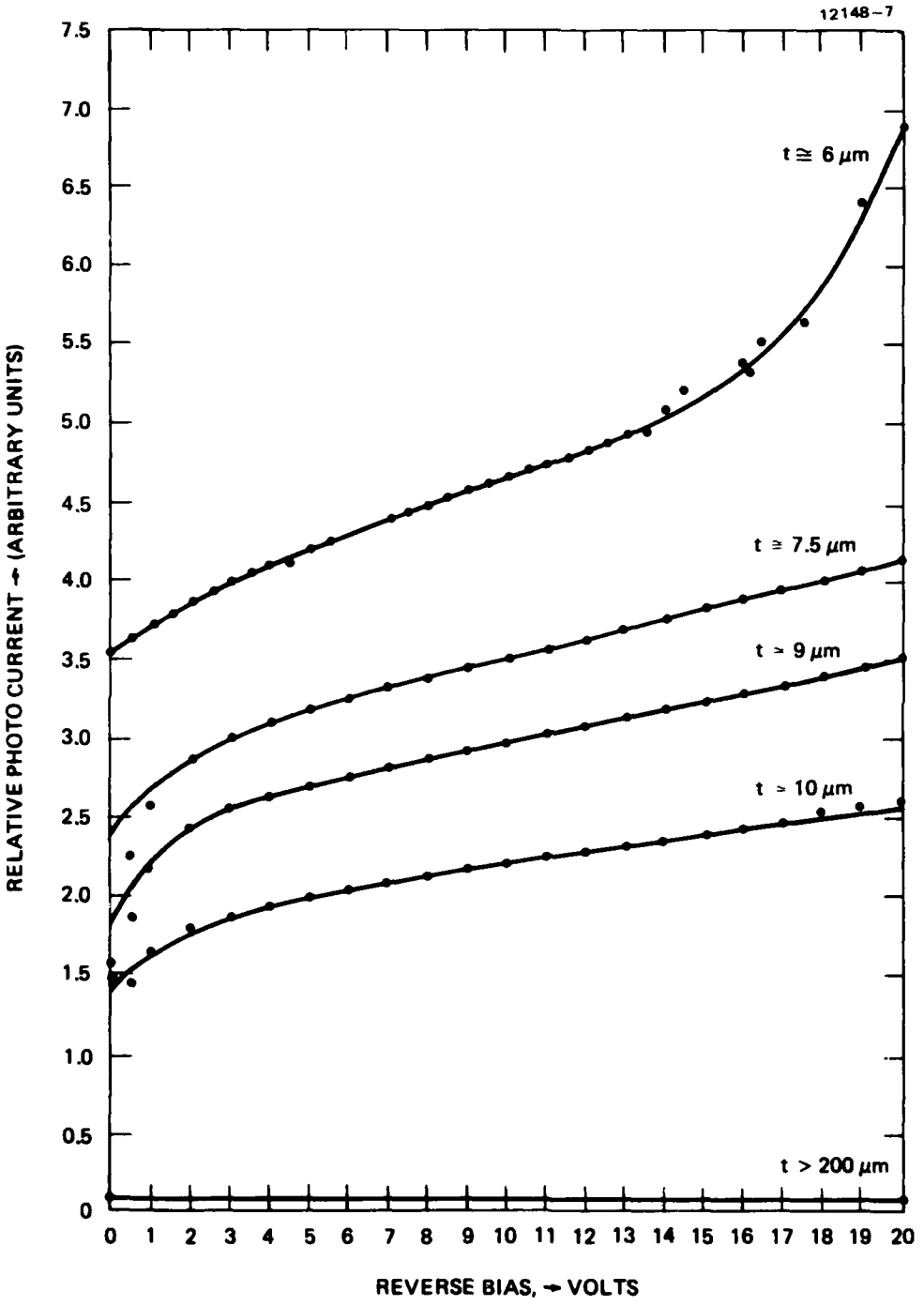

Figure 18. The measured photocurrent from a 400-μm-diameter illuminated (1.152 μm) Schottky diode on p-InP as a function of reverse bias for diodes of various thickness.

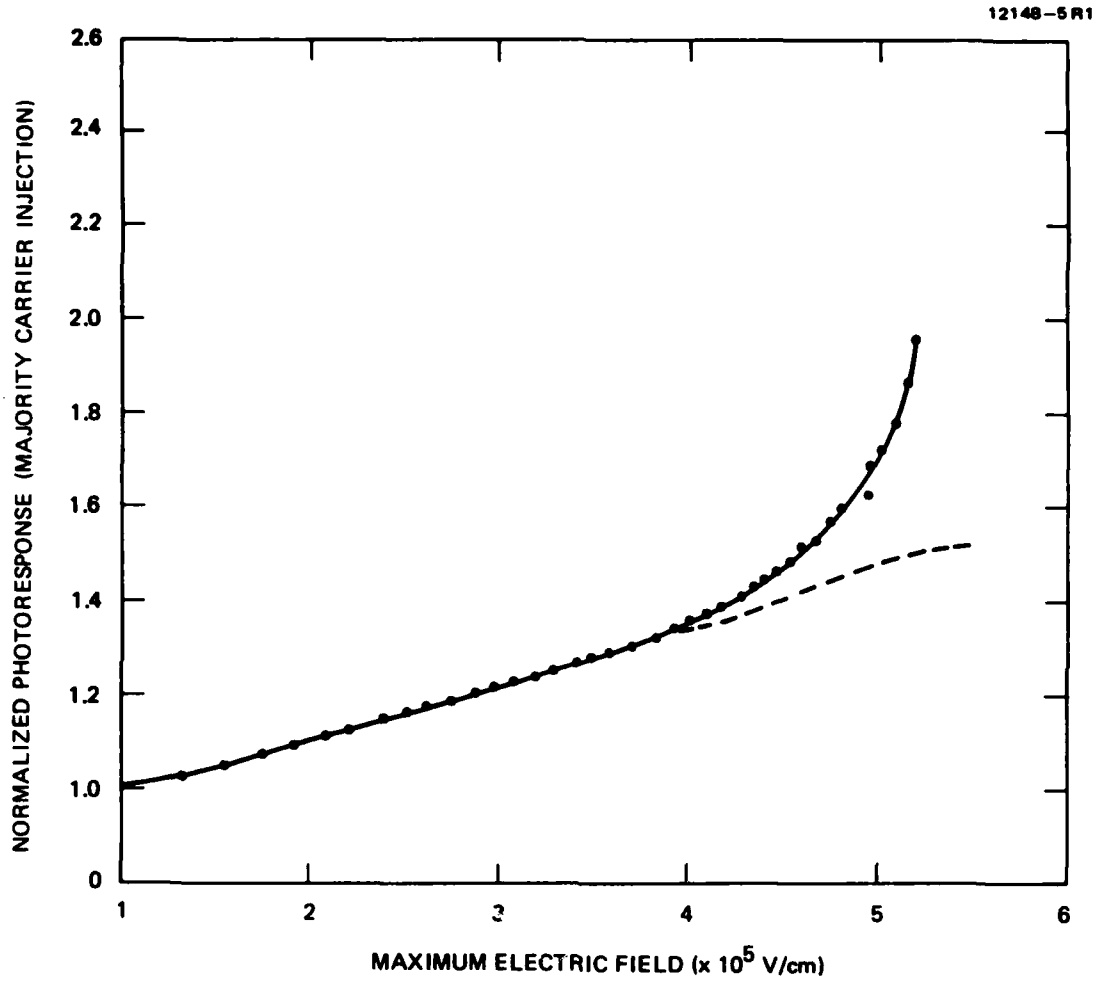

Figure 19. Normalized photocurrent caused by 0.6328 μm illumination on a Schottky diode on p-InP. The dash line represents the estimated base-line photocurrent.

represents the measured normalized photoresponse, while the dash curve represents the estimated base-line photocurrent. We adoped the same procedure first used by Woods[8] to estimate the minority carrier nonmultiplied photocurrent. Since the minority carrier transport is by diffusion, solution of the diffusion equation with the appropriate boundary conditions will be given by Equation (2). We find that best fit to the low field (nonmultiplied) measured photocurrent is obtained using a minority carrier diffusion length of 2 μm. Using this base-line photocurrent, the multiplication factor due to pure electron injection (Mn) can be calculated. The variation of Mn as a function of electric field is shown in Figure 20.

The normalized photoresponse due to majority carrier (hole) injection when the sample is illuminated with 1.152 μm radiation and as a function of electric field is shown in Figure 21. Kao and Crowell[7] have shown that an accurate base-line photocurrent for pure majority carrier injection in Schottky diodes can be obtained by considering quantum mechanical transmission and image force lowering. Under these conditions, the normalized base-line photocurrent is given by Equation (3). In Figure 21, we plot the base-line photocurrent given by (3) for the effective mean free path for photon scattering, $\lambda_e \cong 18\text{Å}$. Using this as the baseline photocurrent, the estimated hole multiplication factor, M_p, is plotted in Figure 22.

D. DISCUSSION OF RESULTS

Using the procedures described above, the variation of the multiplication coefficients due to pure electron and hole injection (Mn and Mp) have been obtained as functions of electric field. From these data, $\alpha(E)$ and $\beta(E)$ can be estimated using Equations (4) and (5), respectively. In Figure 23, we plot the variation of ionization coefficients of electrons (α) and holes (β) as a function of electric field obtained from the present measurements. The data clearly shows that the ionization coefficient of holes (β) is higher than the ionization coefficient of electrons (α). At low electric fields we estimate that β/α varies between 3 and 5.

We compared the results from our study to those obtained by other workers on the variation of α and β as a function of electric field in InP. Almost all available published data is plotted in Figure 24. At low values of electric field our experimental data is in reasonable agreement with that of Kao and Crowell,[7] Stillman et al,[9] and Armiento et al.[10] In fact, over the range of

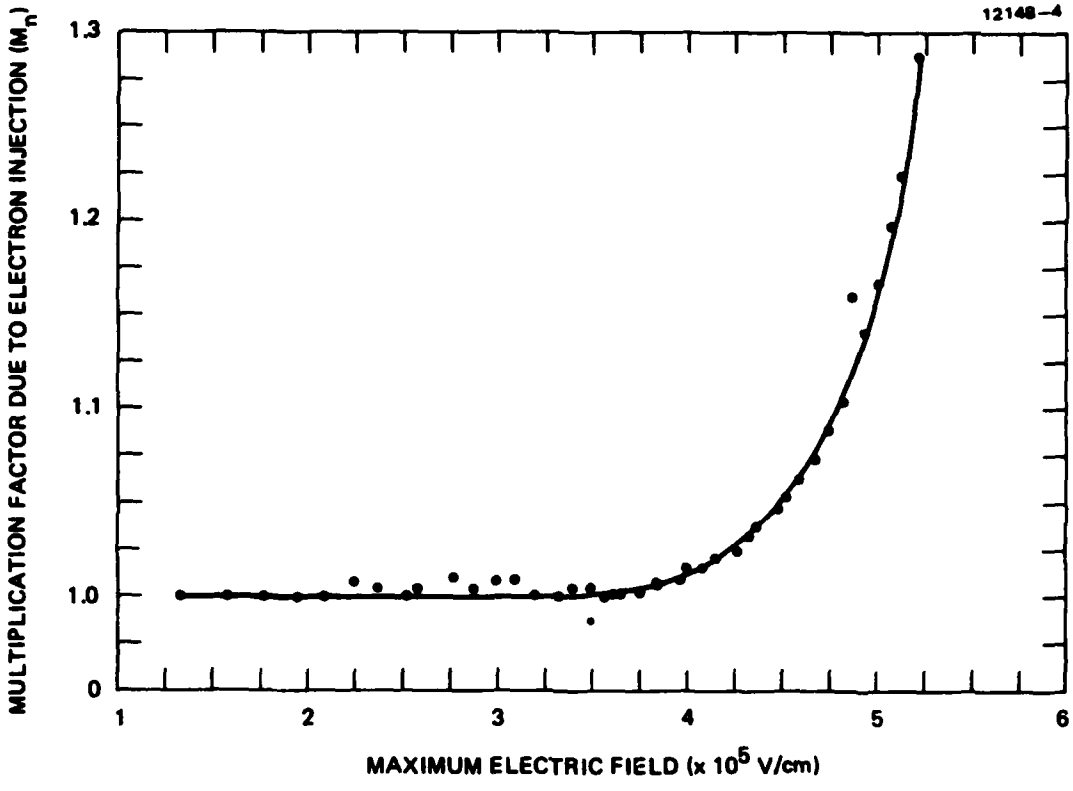

Figure 20. Electron-initiated avalanche multiplication factor (Mn) obtained from a Schottky diode on p-InP as a function of electric field.

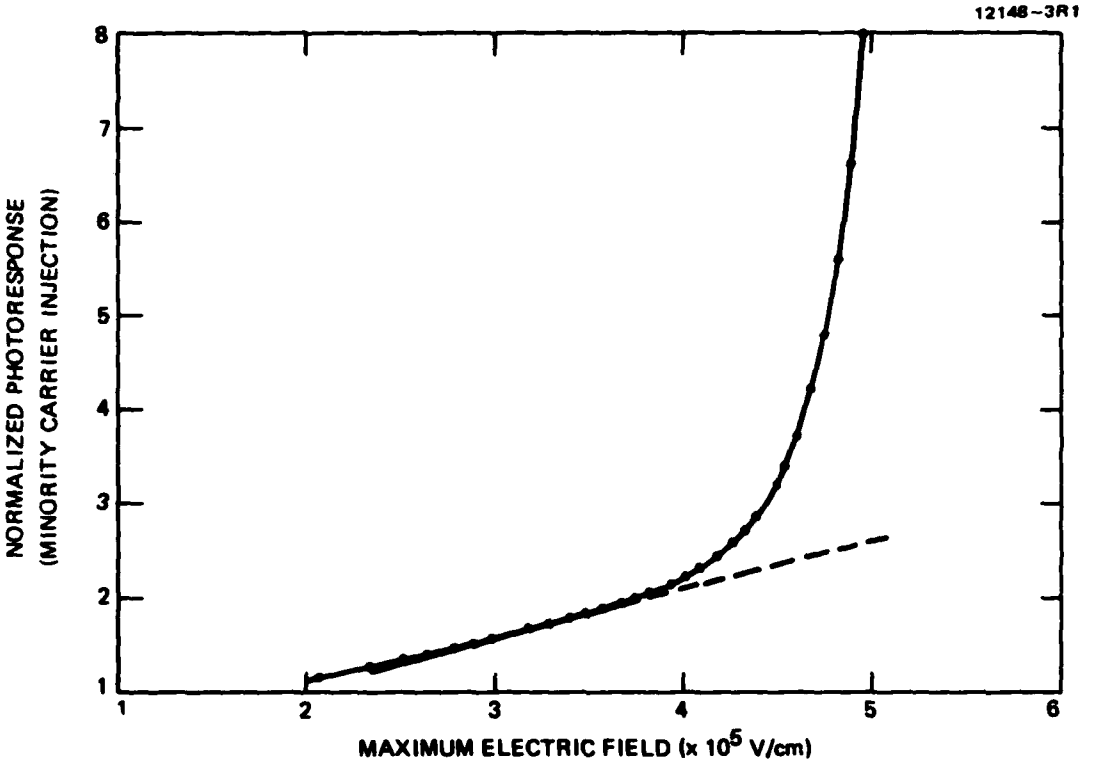

Figure 21. Normalized photoresponse caused by 1.152 μm illumination on a p-InP Schottky diode.

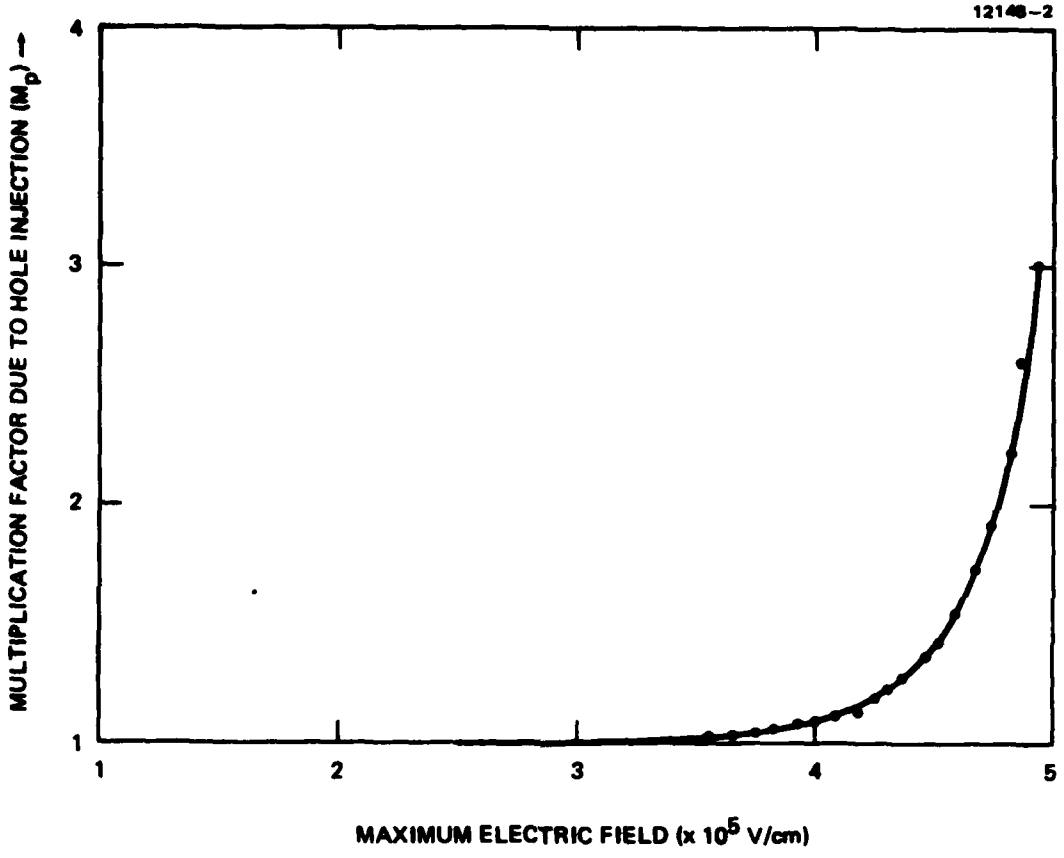

Figure 22. Hole initiated avalanhe multiplication factor (Mp) obtained from a p-InP Schottky diode as a function of electric field.

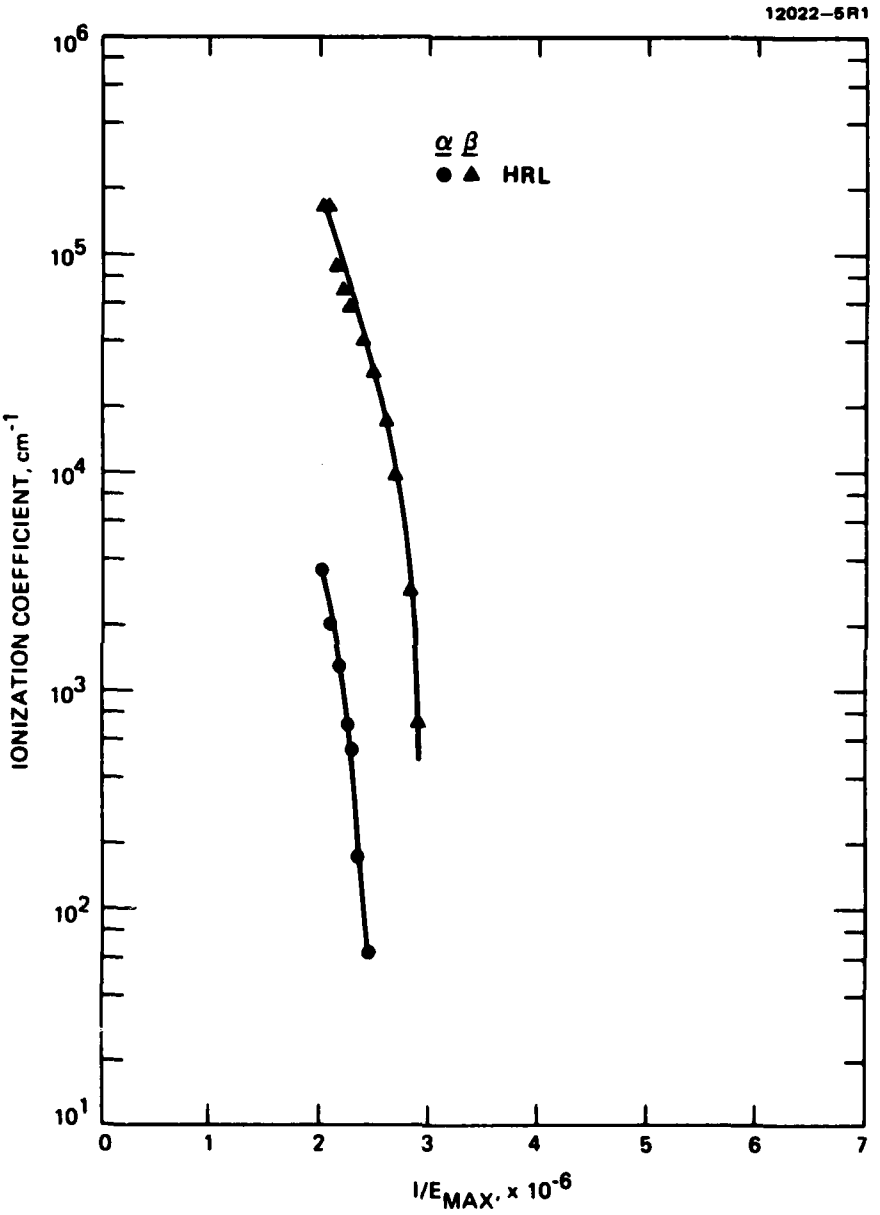

Figure 23. Ionization coefficients (α and β) in InP as a function of the inverse of electric field.

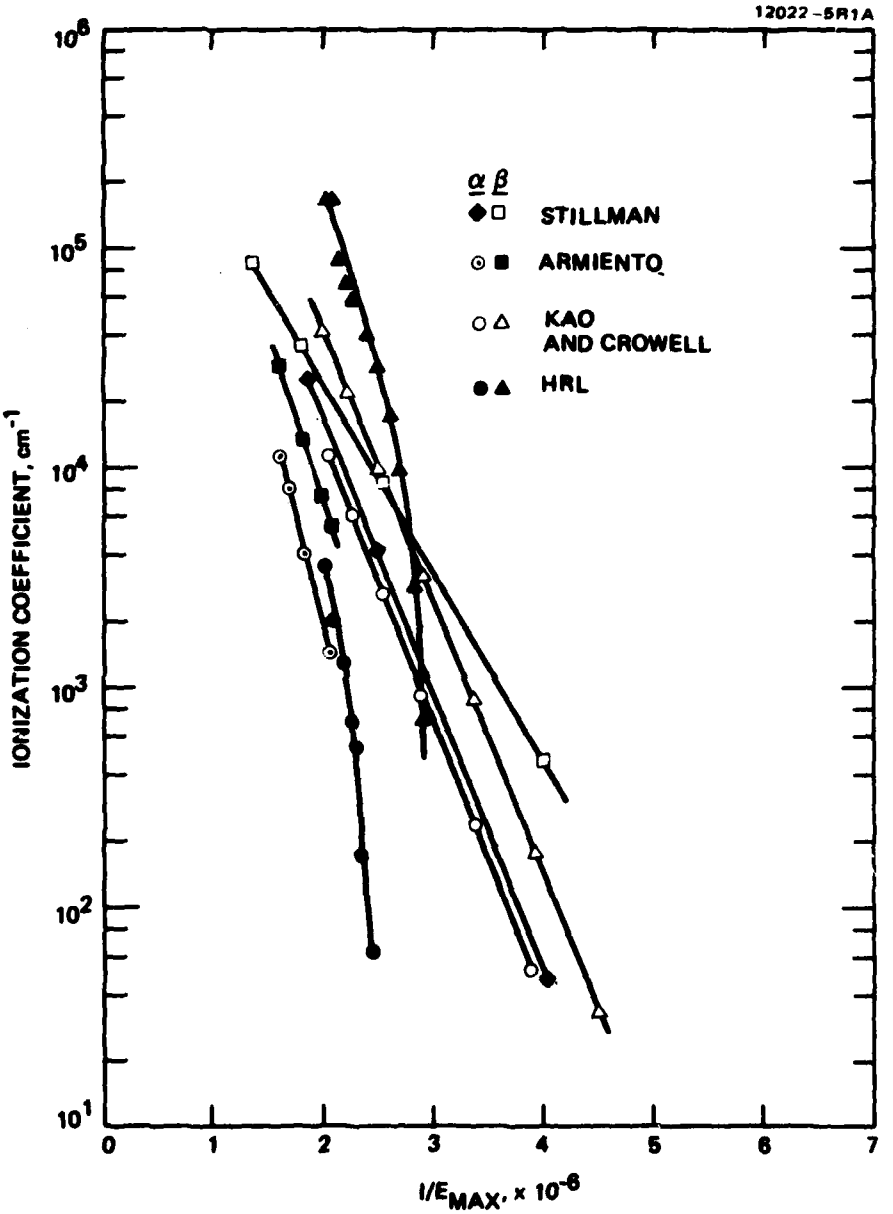

Figure 24. Comparison of the present results from previously published ionization coefficient data on InP as a function of the inverse of electric field.

electric fields studied, the values of α agree reasonably well with other published data. On the other hand, at high values of electric fields, our results tend to overestimate the hole ionization coefficient (β). We believe the primary reason for the discrepancy is due to our underestimating the electric fields in our device structure. There are two plausible causes for this.

First, the surface geometry used in our devices requires an exact two-dimensional solution to estimate the electric magnitude of the fields in the device. Our simplified approach is a 1-dimensional solution to a vertical structure. Secondly, recent deep-level transient spectroscopy (DLTS) measurements performed on the test devices reveal the presence of a hole trap at $\sim$0.44 eV at concentrations of between $2 - 3 \times 10^{15}$ cm^{-3}. The presence of deep-level traps at such high concentrations will have a profound influence on the distribution of the electric fields in the depletion region. In our analysis, we assume a uniform, linear variation of the field in the depletion region. The presence of deep levels will severely distort the field distribution, making such simplified analysis inapplicable. A combination of these two factors can result in underestimating the electric fields encountered in our devices, especially at high fields, and can explain the observed high values of β in high electric fields.

Regardless of the absolute values of α and β, it is clear from the present studies that the ionization coefficient of holes (β) is greater than those of electrons (α) in InP in agreement with most published data.

SECTION 6

SUMMARY

The results discussed in the previous sections of this report are summarized below.

In the area of epitaxial growth, high-purity n-type layers with carrier concentrations of 3×10^{15} cm^{-3} and room temperature mobilities of $\sim$5,000 cm^2 V^{-1} sec^{-1} with excellent surface morphology can be grown reproducibly using the infinite solution growth technique. To grow layers with such properties, it is necessary to introduce small quantities $\sim$(0.1 to 10 ppm) of water vapor in the growth ambient. The presence of water vapor in the growth ambient suppresses the reduction of quartz to silicon by the hydrogen present in the growth ambient. This minimizes the silicon doping of the solution and the epitaxial layers. Auger electron spectroscopy (AES) and secondary ion mass spectrometry (SIMS) measurements show the presence of a higher concentration of Si in the epitaxial layers grown in the absence of water vapor. The SIMS data also reveal the presence of S in these layers. Thus a detailed explanation of the measured electrical and photoluminescence properties of the epitaxial layers involves the interaction between Si and S, the two dominant residual impurities.

Schottky diodes with Al, Ag, and Au as barrier metals were fabricated on highly doped p-type InP by conventional photolithographic techniques. All of these diodes exhibited low leakage currents and abrupt breakdown characteristics. From the I-V characteristics of these devices, we estimate the Schottky barrier heights to be 0.9, 0.74, and 0.64 eV, respectively Al appears to be the best Schottky metal for fabricating test devices for performing ionization coefficient measurements.

A computer-controlled system capable of performing photocurrent measurements as a function of bias has been assembled. The necessary software for performing these automated measurements have been developed. Photoresponse measurements on Al Schottky diodes on p- InP have been performed with both

0.6328 and 1.152 μm illumination. Procedures developed by Kao and Crowell to obtain non-multiplied photocurrents have been applied to the present case. Data obtained from diodes which were thinned by chemical etching techniques reveal both electron- and hole-initiated avalanche multiplication. Analysis of the data shows that over the range of fields studied the hole ionization coefficient (β) is larger than the electron ionization coefficient (α) in InP.

REFERENCES

1. S.H. Groves and M.C. Plonko, Institute of Physics Conference, Series No. 45, p. 71 (1978), and references therein.

2. R.C. Clarke, Institute of Physics Conference Series No. 45, p. 19 (1978), and references therein.

3. J.P. Duchemin, M. Bonnet, G. Benchet, and F. Koeloch, Institute of Physics Conference Series No. 45, p. 10 (1978), and references therein.

4. L. Frass and K. Zanio, J. Electron. Mat. 7, 221 (1978).

5. J.H. McFee, B.I. Miller, and K.J. Bachman, J. of Electrochem. Soc., 124, 259 (1977).

6. A.G. Chynoweth in Semiconductors and Semimetals, R.K. Willardson and A.G. Beer Eds., Vol. 4 (Academic Press, 1968).

7. C.W. Kao and C.R. Crowell, Solid State Electron. 23, 881 (1980).

8. M.H. Woods, W.C. Johnson, and M.A. Lampert, Solid State Electron. 16, 381 (1973).

9. L.W. Cook, G.E. Bulman, and G.E. Stillman, Gallium Arsenide and Related Compounds, 1981, Conference Series 63, pp. 281-286, Institute of Physics: Bristol and London.

10. C.A. Armiento, S.H. Groves and C.E. Huriwtz, Appl. Phys. Lett. 35, 332 (1979).

blank

DISTRIBUTION LIST

Commander
Naval Air Systems Command
ATTN: AIR-310B (Mr. James Willis) (5 cys)
AIR-00D46 (14 cys)
Washington, DC 20361

Commander
Naval Ocean Systems Center
ATTN: Dr. A. Clawson/Code 922
San Diego, CA 92152

RCA
David Sarnoff Research Cent
ATTN: Dr. G. H. Olsen
Princeton, NJ 08540

MIT
Lincoln Laboratory
ATTN: Dr. J. J. Hsieh
Dr. A. G. Foyt
P.O. Box 73
Lexington, MA 02173

Office of Naval Research
ATTN: Dr. Larry Cooper/Code 427
800 N. Quincy Street
Arlington, VA 22217

Commander
US Army Research Office
ATTN: Dr. H. Wittman
P.O. Box 12211
Research Triangle Park, NC 27709

Advisory Group on Electron Devices
ATTN: Working Group "A"
201 Varick Street
New York, NY 10014

Dr. Roy Potter
1017 17th Street
Bellingham, WA 98225

Varian Associates
Solid State Laboratory
ATTN: Dr. S. B. Hyder
611 Hansen Way
Palo Alto, CA 94303

The University of Michigan
Electron Physics Laboratory
Department of Electrical & Computer Engineering
ATTN: Prof. Brenton L. Mattes
Ann Arbor, MI 48109

Commanding Officer
Naval Research Laboratory
ATTN: Dr. Howard Lessoff/Code 6820
Washington, DC 20375

Colorado State University
Department of Electrical Engineering
ATTN: Dr. Kenneth A. Jones
Fort Collins, CO 80523

Stanford University
Stanford Electronics Laboratory
ATTN: Prof. Gerald Pearson
Stanford, CA 94305

Massachusetts, Institute of Technology
Department of Electrical Engineering
and Computer Sciences
ATTN: Prof. Clifford Fonstadt
Cambridge, MA 02139

North Carolina State University
Electrical Engineering Department
ATTN: Dr. M. Littlejohn
Raleigh, NC 27650

University of California, San Diego
Department of Electrical Engineering
and Computer Sciences
ATTN: Prof. William Chang/MS C014
La Jolla, CA 92023

ATTN: Dr. Harry Wieder

University of Utah
Department of Electrical Engineering
ATTN: Dr. Gerry Stringfellow
Merrill Engineering Bldg.
Salt Lake City, UT 84112

Cornell University
Department of Electrical Engineering
ATTN: Prof. Lester Eastman
Ithaca, NY 14850

University of Colorado
Department of Electrical Engineering
ATTN: Dr. Aroldo Majerfeld
Boulder, CO 80309

University of Illinois
Department of Electrical Engineering
ATTN: Prof. Greg Stillman
Urbana, IL 61801

Rockwell International
Electronics Research Group
ATTN: Dr. D. Dapkus
P.O. Box 3105
Anaheim, CA 92803

CRYSTA COMM, Inc.
ATTN: Dr. George Antypas
486 Ellis Street
Mountain View, CA 94043


DATE
ILME